TEKNILLINEN TIEDEKUNTA / FACULTY OF TECHNOLOGY

HYDROTHERMAL ALTERATION OF THE KEMI LAYERED INTRUSION

Fabian Mauricio Botello Becerra

DEGREE PROGRAMME OF ECONOMIC GEOLOGY

Master's thesis

April 2019

ABSTRACT

FOR THESIS University of Oulu Faculty of Technology

Degree Programme (Master's Thesis) Degree programme in Economic Geology		Major Subject (Licentiate Thesis) Geology and Mineralogy	
Author Botello Becerra, Fabian Mauricio		Thesis Supervisor Sheng-Hong Yang	
Title of Thesis Hydrothermal alteration of the Kemi layered intrusion			
Major Subject Geology and Mineralogy	Type of Thesis Master's thesis	Submission Date April, 2019	Number of Pages 81 pp, 18 appendixes

Abstract

The Kemi chromite deposit is located near the towns of Kemi and Tornio (northern Finland). The mineralization is hosted within the mafic-ultramafic Kemi intrusion (~2.4 Ga) that is part of the Tornio – Näränkävaara belt. The main chromite zone is located in the basal part of the intrusion and is enveloped and intercalated by peridotites and bronzites. Hydrothermal alteration has pervasively affected the intrusion mainly in the lower and upper segments, leaving the middle part relatively unaltered. These lithologies can still be identified due to the preservation of their primary textures. The altered ultramafic lithologies had been previously catalogued as cumulate, chlorite, amphibole, serpentine and pyroxene peridotites, amphibole and talc pyroxenites, and serpentinites. Further petrographic observations suggest that the ultramafic rocks experienced at least six episodes of hydrothermal alteration that lead to the replacement of primary minerals to assemblages of serpentine, chlorite, amphibole, carbonate and talc. Evidences in the petrography and mineral chemistry suggests the alteration fluid evolve towards more silica rich compositions.

The hydrothermal fluids responsible for Kemi intrusion alterations can be related to the metamorphism of the footwall rocks during the Svecofennian Orogeny.

Variations in alteration patterns and mineralogy as well as variations in the mineral chemistry do not correlate with the proximity to the chromitite ore zone.

Additional Information

TABLE OF CONTENTS

1 INTRODUCTION

The 2.44 to 2.5 Ga mafic layered intrusions in the Tornio-Näränkävaara belt are located at the contact between the Archean basement rocks and the Proterozoic volcano-sedimentary Supracrustal schist belts (Peräpohja and Kuusamo; Fig. 1). The origin of these magmatic intrusions is assigned to a mantle plume flare up in a continental rifting environment (Iljina and Hanski, 2005; Yang et al., 2016).

The mafic-ultramafic magmatic complexes of the Tornio-Näränkävaara belt contain variable styles of mineralization including chromite, base metal sulfides, PGE, vanadium bearing magnetite. Currently, only the chromitite deposit in the Kemi intrusion is under exploitation (Iljina and Hanski, 2005). The Kemi intrusion in this belt is characterized by peridotitic layers in its basal portion grading stratigraphically upwards to pyroxenitic, gabbroic and anorthositic rocks (Alapieti et al., 1989; Alapieti and Huhtelin, 2005; Huhtelin, 2015). Extensive alteration is found in the lower and upper portions of the intrusion. The mineralization was discovered by GTK in 1960 following the reports of a local prospecting enthusiast. Exploration was carried afterwards by Outokumpu defining 30 Mt of ore in the basal layers of the intrusion (Alapieti et al., 1989). The mine is located nearby the town of Kemi at 28 km away from the port town of Tornio. Mine operations started in 1965 as an open pit and shifted to underground mining in 2006 (Alapieti and Huhtelin, 2005). Currently, the proven ore reserves are 36.8 Mt, 25.9 % Cr_2O_3 with Cr/Fe ratio of 1.7. Measured, indicated and inferred resources are 3.3 Mt, 88.5 Mt and 26.2 Mt, respectively (Huhtelin, 2018; personal communication).

Previous research on the Kemi intrusion and the chromitite deposit has focused on questions related to the magmatic processes responsible for the mineralization and genesis of the intrusion. Such works include the following. Alapieti et al., (1989) is probably the most important paper, always referenced by later studies on Kemi intrusion. It consolidates different aspects of Kemi intrusion geology: distribution and geometry of the intrusion, layers and ore, rock types from different stratigraphy and their representative mineralogy, and geochemistry, and remarks on the genesis of the intrusion and the chromitite mineralization. Further works such as Alapieti and Huhtelin (2005), and Huhtelin (2015) update the aforementioned aspects with valuable information. Yang

et al., (2016) contemplate the origin of the ultramafic intrusions in the Fennoscandian Shield as the emplacement of plume related magmatism, based on Re – Os and Nd – Sr isotope studies. Vasilopanagos (2016) MSc. thesis registers different magma replenishment events in Kemi intrusion, based on the variations of Mg# in olivine and pyroxene.

A substantial portion of the host rock to the ore are altered to serpentinites, chlorite-rich peridotite, and talc (carbonate) rocks, indicating substantial hydrothermal alteration. The timing and conditions of the alteration events are unconstrained, as well as the origin of the fluids involved. Hydrothermal alteration of Kemi's rocks has been only briefly mentioned in previous works (e.g. Alapieti et al., 1989). Nonetheless, the most reliable (and probably the only) source of information about this alteration is Grönholm (1994), which includes petrographic descriptions and classifications envisaging hydrothermal alteration of the ultramafic peridotites that hosts the Kemi chromitite ores.

Hence, this project aims to investigate the different types of alteration in the Kemi intrusion with the goal to define timing relationships, the spatial distribution of the alteration types in relation to the ores, the compositional variations and element mobility during alteration. Such data may be useful as a geochemical vector in exploration since alteration halos can be spatially extensive and might also be detectable in secondary dispersion halos.

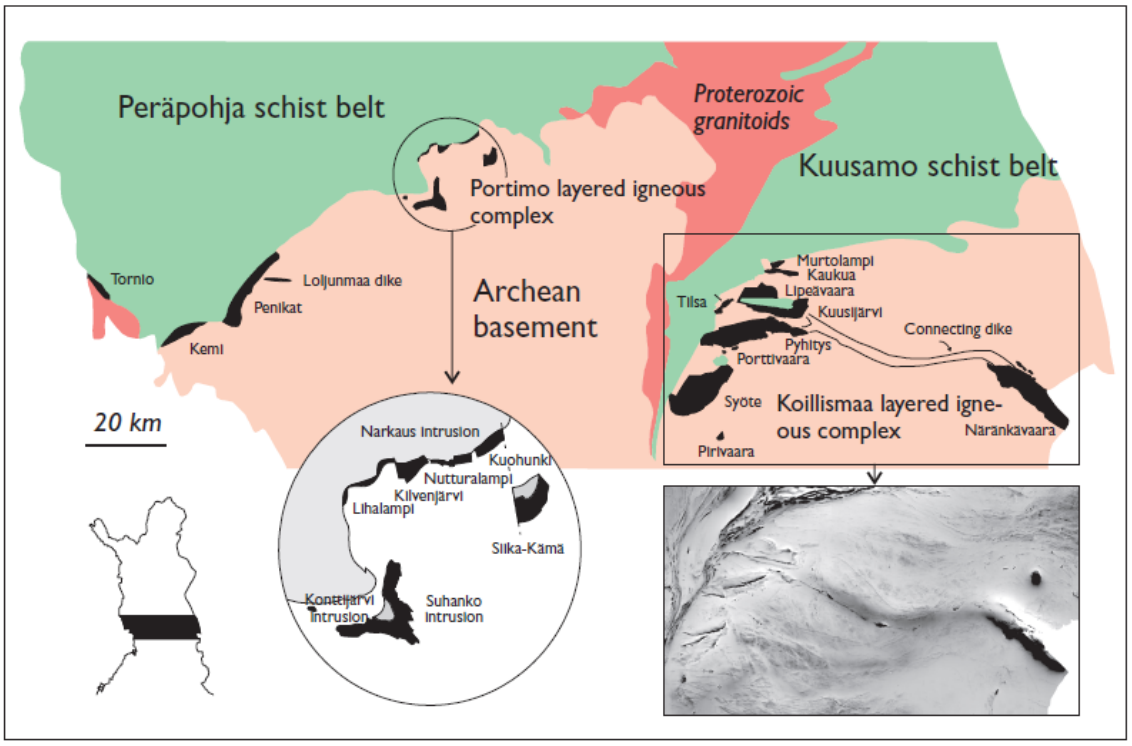

Figure 1. Layered intrusions of the Tornio – Näränkävaara belt (black). In the lower right-hand corner the connecting dike of the Näränkävaara intrusion is evidenced in the low altitude aeromagnetic map (from Iljina and Hanski, 2005). Published with permission from Elsevier.

1.1 Chromitite mineralization in layered intrusions

Occurrences of chromite ore are defined by two types of deposits: podiform chromitite in ophiolite and stratiform chromite in mafic layered intrusions. Podiform chromitite is formed in subrasubduction zones, in the ultramafic portions of ophiolites, hosted in harzburgites, lherzolites and occasionally dunites and wehrlite (Cawthorn et al., 2005; Mosier et al, 2012). Although much smaller in size and tonnage, compared to layered intrusions related chromitite, their importance lies in the presence of refractory chromite (Cawthorn et al., 2005). Layered intrusions are formed in different crustal levels from intrusions of mafic magma, which commonly develop stratiform patterns similar to those in sedimentary rocks.

The development of layering in mafic intrusions has been attributed to two types of processes: dynamic and non – dynamic. Dynamic processes involve mechanical sorting (crystal settling and magma currents), convection, magma injection and mixing (responsible for the formation of chromitite layers), liquid immiscibility and fluid migration in a crystal mush. Non – dynamic processes include changes of intensive

parameters of crystallization, processes of equilibration in the crystal and modal and cryptic layering due to chemical diffusion in the crystal mush. Nonetheless, the occurrence of layering can seldom be attributed to only one process (Namur et al., 2015).

The formation of chromitite layers in mafic intrusions in still under debate. Different models have been proposed (Namur et al., 2015 and references therein), although no single model can account for all the features. The most accepted hypothesis for the formation of chromitite layers is the mixing of primitive and fractionated magmas which drive the composition of the mixed magma to the stability of chromite (Irvine, 1975), or mixing between a mafic magma with a felsic melt by crustal contamination (Irvine, 1977). Alternatively, co-crystallization of chromite together with mafic minerals followed by density sorting due to subsidence of the central portion of magma chamber is proposed by Maier et al. (2008, 2013). Another model is co-crystallization of chromite together with mafic minerals in a deeper staging magma chamber followed by injection of crystal slurry into an upper chamber, and there is density sorting in the dynamic flow of crystal slurry. One difficulty for a closed system process is the large amount of magma volume to produce the observed chromitite is far more than the observed magmatic rocks related to the chromitite (Eales, 2002). Cawthorn and Walraven (1998) suggest that the residual magma was pushed outward by the new injection(s) of magma.

Layered intrusions host the most important resources of Cr, PGE and V in the world. The most prominent and representative occurrence of this kind is the Bushveld complex in South Africa (Cawthorn, 2015). The Bushveld complex (2.06 Ga) is composed of layers from ultramafic in the bottom to monzonitic composition towards the top. The complex is located in the Kaapvaal craton, hosted by quartzites, argillites and dolomites of the Transvaal Supergroup. The maximum thickness of the Bushveld intrusion is of about 8 km and has an exposed area of 40,000 km^2. The Bushveld complex is roughly divided in the Marginal zone (in contact with the footwall; noritic compositions), Lower Zone (orthopyroxenites – dunites), Lower Critical Zone (chromitite, orthopyroxenites), Upper Critical Zone (chromitite, orthopyroxenites, norite and anorthosite rhythmic units; host of the Merensky Reef), Main Zone (gabbronorite) and Upper Zone (gabbro, olivine – diorite, anorthosite, magnetite; Naldrett et al., 2012; Scoon and Mitchell, 2012; Cawthorn, 2015). Chromitite layers in the Bushveld Complex can extend up to more than 100 km along strike. Chromitite in Bushveld is mainly hosted in the Critical Zone. There are roughly 13

chromitite layers which are divided in three groups; Lower Group (LG-1 to LG-7), Middle Group (MG-0, MG-1, MG2a-b-c, MG-3, MG-3a, MG-4 and MG-4a) and the Upper Group (UG-1 and UG-2; Fig. 2).

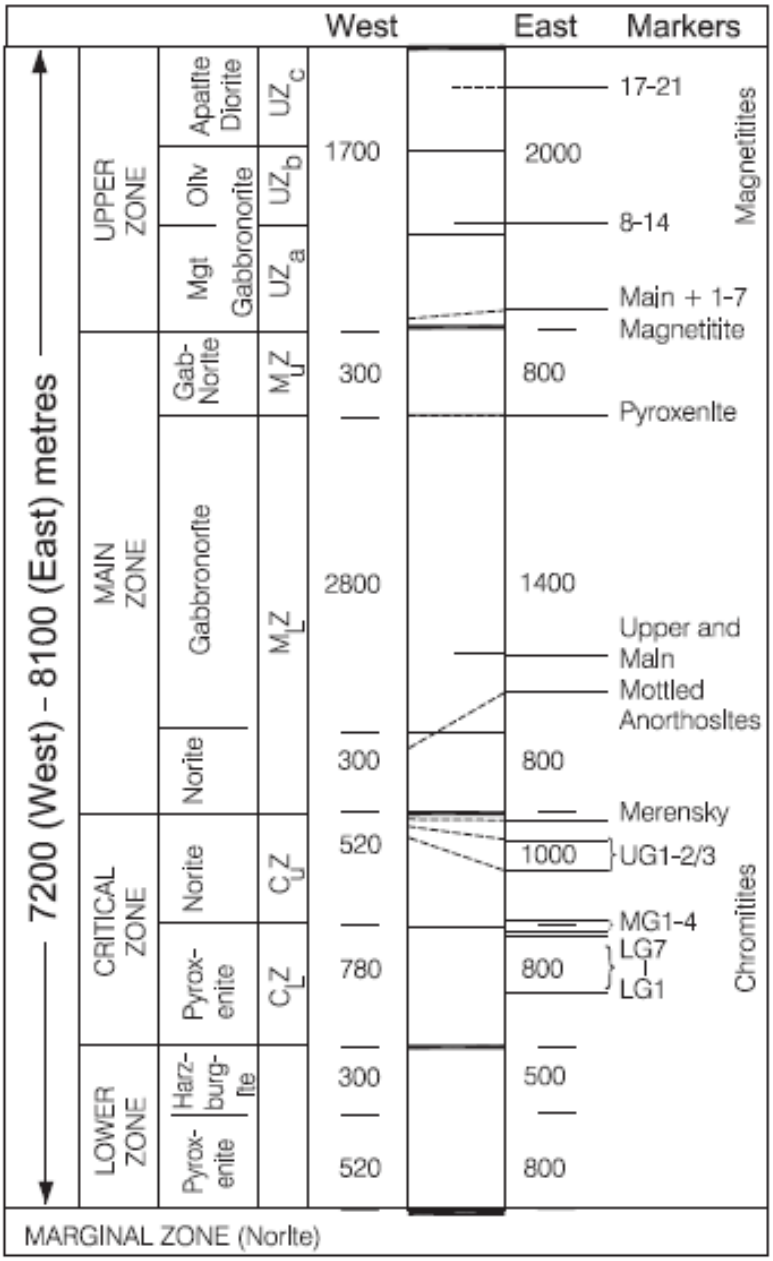

Figure 2. Bushveld Complex stratigraphic column. From Cawthorn et al., (2005).

Another important layered intrusion is the Stillwater Complex (Fig. 3), Montana (USA). The Stillwater Complex (2.7 Ga) is emplaced in a sequence of metasedimentary rocks. The complex is exposed for about 50 km along strike with a thickness of approximately 6.5 km. The intrusion is divided, from base to top, into Basal series (~100 m thickness; orthopyroxenites and gabbronorites), Ultramafic series (~2 km thickness; cyclic

harzburgites – pyroxenite) and the Banded series (~4 km thickness; norite, gabbronorite and anorthosite). The Stillwater Complex contains PGE mineralizations in the Lower Banded series as well as chromite mineralizations in the Peridotite zone of the Ultramafic series (Cawthorn et al., 2005; Lenaz et al., 2012). The origin of chromitites in the Stillwater Intrusion has been attributed to multiple magma injections of different magma types based on geochemical and isotopic variations (Lenaz et al., 2012 and references therein).

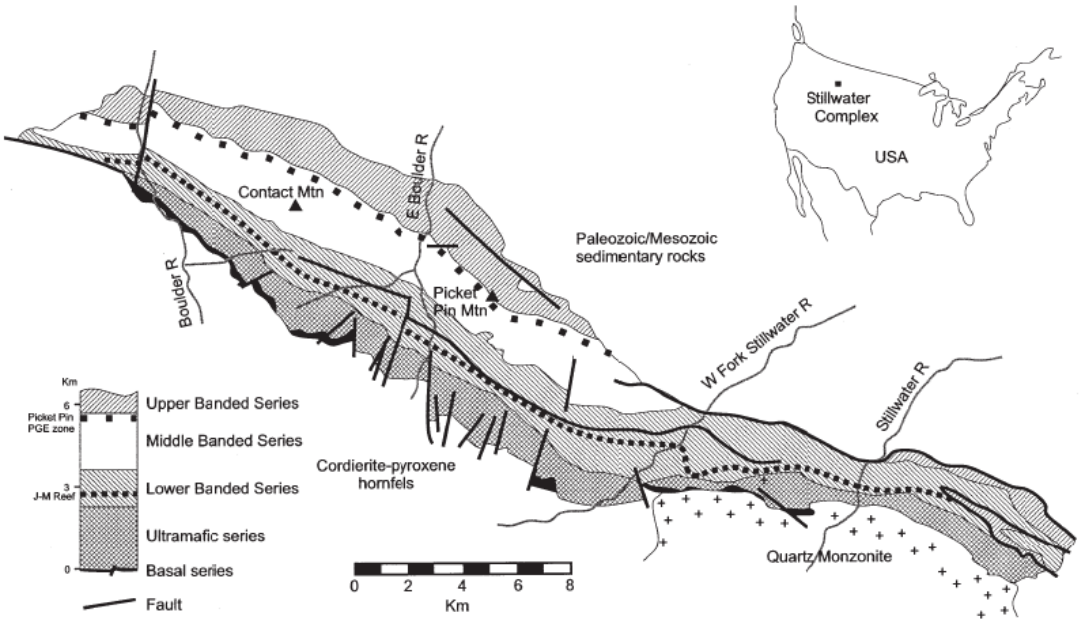

Figure 3. Stillwater Complex geological map and stratigraphical column. From Cawthorn et al., (2005).

The Kemi intrusion is another representative layered intrusion. Kemi mine is currently the only operating chromium mine in Europe. Different processes are accounted for the formation of Kemi chromitites. These processes include magma contamination by footwall rocks. This is evidenced by the presence of granitic veins in the base part, the occurrences of xenoliths from basement and alkali rich inclusions in chromite. Multiple injections of fresh magma and slumping may also have played role for the increased thickness in the central part of the intrusion (Alapieti et al., 1989).

1.2 Serpentine textures

Serpentine alteration is probably the most abundant and widespread in peridotites of the Kemi intrusion, hence understanding its occurrences and different textures was crucial for this work. Recent studies of hydrothermal alteration in ultramafic igneous rock have

different approaches e.g., establishing relations and remobilization processes of platinum group elements (Polovina et al., 2004; Li et al., 2008 and references therein) or defining interactions between exhumed peridotites in slow spreading oceanic ridges and sea water (Bach et al., 2004; Paulick et al., 2006; Alt et al., 2007; Roumejón and Cannat, 2014; Roumejón et al., 2015). In previous years, the research interest was also focused on the crystallography and different types of serpentines produced by hydrothermal alteration (Wicks and Whittaker, 1977; Wicks and O'Hanley, 1988). These works specified the classification of serpentines.

Serpentine textures are classified to pseudomorphic, non-pseudomorphic and vein textures (Wicks and Whittaker, 1977). Pseudomorphic textures are formed by direct replacement of olivine to serpentine. Pseudomorphic textures in olivine are usually represented as mesh textures (development of altered fragments and fractures, causing a "mesh" appearance) and hourglass textures (replacement of the grain leaving "hourglass" shaped aggregates). Pyroxenes are mostly altered to bastites (serpentine pseudomorphs of interference colors up to the first order) with fibrous to almost featureless appearance (Wicks and Whittaker, 1977). In rare cases, pyroxene might develop mesh textures.

Non-pseudomorphic textures are developed by recrystallization of pseudomorphic serpentine and less commonly by direct replacement of the primary minerals to serpentine (Wicks and Whittaker, 1977). Non-pseudomorphic textures are characterized by aggregates of elongated anhedral serpentine with interpenetrating and/or interlocking textures.

Interpenetrating textures are formed by the development of isolated flakes of serpentine which start to interfere with each other as crystallization proceeds. Interlocking textures are produced by segregated patches of equant, irregular grains of serpentine in a tight interlocking fabric, which are later joined together by further recrystallization (Wicks and Whittaker, 1977).

Serpentine veins can be formed in fractures, joints and shears. These veins are classified as chrysotile asbestiform and non-asbestiform (any other occurrence besides asbestiform; e.g. banded, interpenetrating texture, featureless; Wicks and Whittaker, 1977).

Some of the above-mentioned features can be used to identify the serpentine mineralogy. In Wicks and Whittaker (1977), it is recognized that the most common types of serpentine in pseudomorphic are lizardite, and antigorite in non-pseudomorphic. Another accessible way to identify serpentine varieties is the use of a gypsum plate to determine the sign of elongation (fast or slow ray) of the serpentine crystal. A classification table can be found in Wicks and O'Hanley (1988), which compiles the texture and optical characteristics of serpentine crystals (Table 1).

Table 1.Identification of serpentine variety based on texture and optical characteristics. From Wicks and O'Hanley (1988)

Texture	Optical Characteristics	Mineralogy
	Pseudomorphic	
Mesh rim	length-fast	lizardite
	length-slow	chrysotile
Mesh center, fine grained	isotropic	lizardite, antigorite or chrysotile
Mesh center, hourglass	length-fast	lizardite
	length-slow	chrysotile or antigorite
Hourglass	length-fast	lizardite
Ribbon	length-fast	lizardite
	Non-pseudomorphic	
Transition	isotropic	lizardite, chrysotile or antigorite
Interlocking	length-fast	lizardite
	length-slow	antigorite, chrysotile or lizardite
Serrate veins	length-fast	lizardite
	length slow	antigorite, chrysotile or lizardite
Interpenetrating	length slow	antigorite, rarely chrysotile or lizardite

2 REGIONAL GEOLOGY

The Tornio – Näränkävaara belt is emplaced within the Karelian domain in the Fennoscandian Shield. Associated intrusions span a distance of about 300 km from Sweden (Kukkola Intrusion) extending eastwards across Finland to Russia (Alapieti et al., 1989; Iljina and Hanski, 2005). The intrusions in Finland are distributed from the west to the east including the Tornio-Kemi-Penikat, Portimo and Koillismaa Complexes with the age of about 2.44 Ga (Iljina and Hanski, 2005). This belt was formed by the ascent of a mantle plume and rifting which might have also led to the break-up of the Late Archean

supercontinent (Alapieti and Huhtelin 2005, Yang et al., 2016).

Extension and vertical - brittle faulting separated the intrusions into different blocks. Uplift of the relatively shallow intrusions partly produced unroofing and erosion of the top-most layers (Iljina and Hanski, 2005). Over this erosional surface, polymictic conglomerates were deposited forming the widely recognized “sedimentary caps” of the complex. Deformation of the belt is associated to the different stages of the Svecofennian Orogeny (1.9 - 1.8 Ga; Alapieti et al., 1989; Grönholm, 1994; Iljina and Hanski 2005). Initially the layered intrusion was tilted from its initial stage. Further deformation led to the metamorphism (greenschist to amphibolite facies) and hydrothermal alteration, being stronger in the western and central parts. In some rocks, primary features have been obliterated by the replacement to secondary minerals. Although altered up to 100%, alteration minerals over these rocks still preserve cumulatic textures, making it possible to estimate mineral compositions(Iljina and Hanski, 2005; Alapieti and Huhtelin, 2005).

The footwall of the intrusions is the Archean gneiss and the hanging wall are Paleoproterozoic schist belts, with the exception of the Näränkävaara intrusion in the Koillismaa Complex (Fig. 1; Iljina and Hanski, 2005). Deposition of the hanging wall supracrustal sequences occurred over an angular discontinuity with the layered intrusions, indicating a shallow depth of emplacement for the complex and a fast uplift and erosion.

The intrusions are broadly composed of a basal marginal series and overlying layers of specific characteristics for each intrusion (layering with or without cyclic units). Two marginal series are defined in the terms of thickness; one is thin (<20 m) consisting of a non-cumulate gabbro followed by bronzitic cumulates and the other one is considerably thicker (>150 m) formed by layers of olivine cumulates, pyroxene cumulates and gabbroic rocks. The overlying layers are composed of ultramafic and mafic sequences and in some intrusion even a topmost layer of granophyre has been identified (Iljina and Hanski, 2005).

Different styles of mineralization are recognized in the Tornio – Näränkävaara belt; chromitite layers in the Kemi intrusion, PGE mineralizations in the Penikat intrusion, Portimo Complex (Suhanko, Konttijärvi, and Narkaus intrusions) and the Koillismaa Complex, and Ti-V iron oxide mineralization in the Porttivaara Block (Koillismaa

Complex, Mustavaara mine). Nonetheless, the only active chromite mine is in the Kemi intrusion (Fig. 4; Alapieti and Huhtelin, 2005; Iljina and Hanski, 2005).

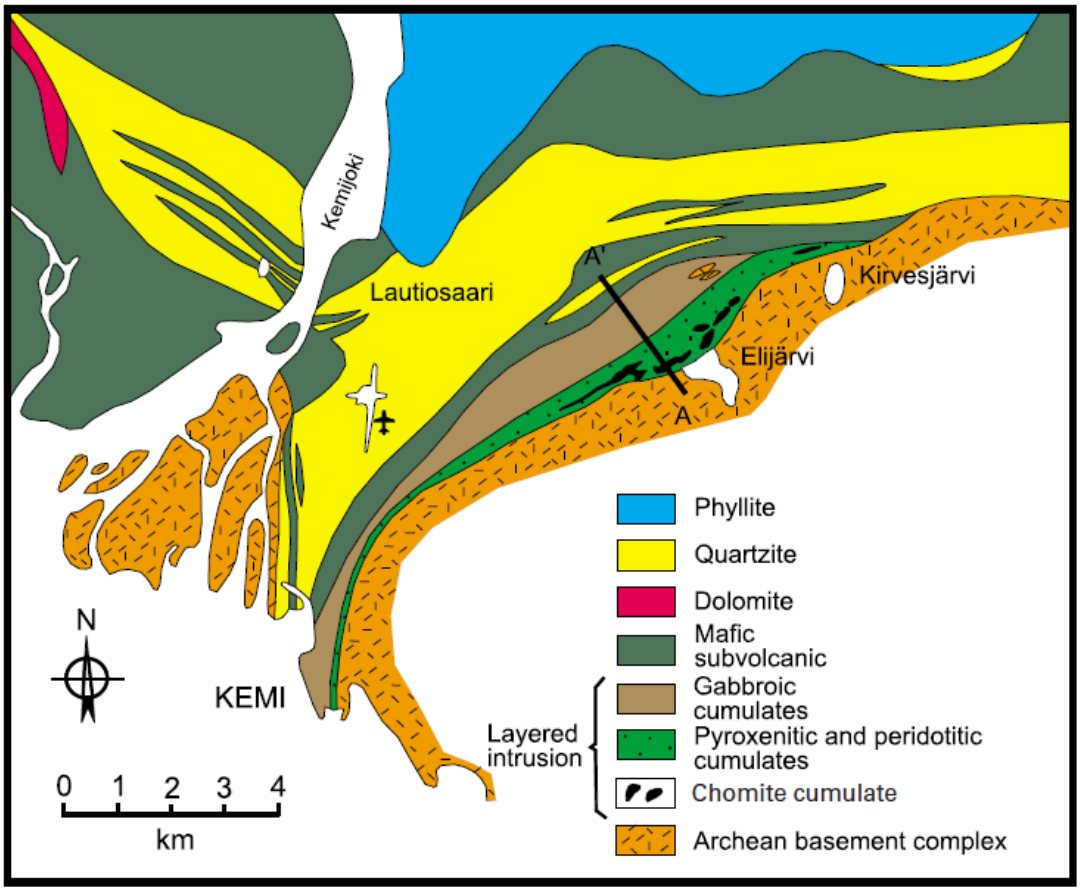

Figure 4. Geological map of the Kemi area. The Kemi layered intrusion has a lensoidal shape with the main mineralization located in the central portion. The profile (A-A') is shown in Figure 5 (from Alapieti and Huhtelin, 2005). Published with permission from Elsevier.

The footwall and hanging wall of the Kemi Intrusion are the Pudasjärvi Complex and the Peräpohja Schist Belt (respectively). The Pudasjärvi Complex is characterized by granite and amphibolite gneisses, granulites, remnants of greenstone schist belts and intrusions of felsic and mafic composition. The ages in the Pudasjärvi Complex span from 3.5 to 2.7 Ga (Lauri et al., 2011; Muttanen and Huhma, 2003; Vaasjoki et al., 2005). The Peräpohja Schist Belt (~2.3 Ga) lays on top of the Archean basement and partly over layered intrusions. The belt is formed by metasedimentary rocks (conglomerates, arkosites and quartzites) and metavolcanic rocks (mostly mafic). The belt is also intruded by rocks of the Haparanda Suite. The degree of metamorphism in the belt is low (greenschist facies) and increases in the north (up to amphibolite facies; Laajoki, 2005; Perttunen and Vaasjoki, 2001; Lauri et al., 2011). In the vicinities of Kemi intrusion (less than 10 Km

to the W-NW), plutonic rocks of the Haparanda Suite are found (Grönholm, 1994). The Haparanda Suite intrusions are located in the surrounding areas of the Finnish-Swedish border and span a wide range of compositions from monzonitic to trondjhemitic and even gabbroic (Hanski and Huhma, 2005). Their ages are of about 1.89 – 1-86 Ga and they are considered to be synorogenic of the Svecofennian Orogeny.

The Kemi intrusion was originally funnel-shaped, but it was tilted during the Svecofennian Orogeny to its present lenticular shape, dipping 70° to the NW (Fig. 5). The intrusion was fragmented into different blocks by faults. Nevertheless, layering in the Kemi intrusion remained subparallel even after deformation. The surface length of the intrusion is around 15km and the width about 0.2-2km, being thicker in the central part and thinner towards the margin (Alapieti et al., 1989; Alapieti and Huhtelin, 2005; Iljina and Hanski, 2005). The feeder dike of the intrusion can be found 260 m beneath the present day surface under the thickest part of the intrusion. The dike is approximately 20 m thick and it is composed of fine grained uralitized rocks at the margins, grading to coarser grained to the center. The rocks are chlorite schists and talc-carbonate rocks. The center of the dike is composed of massive chromitites (Alapieti and Huhtelin, 2005; Huhtelin, 2015).

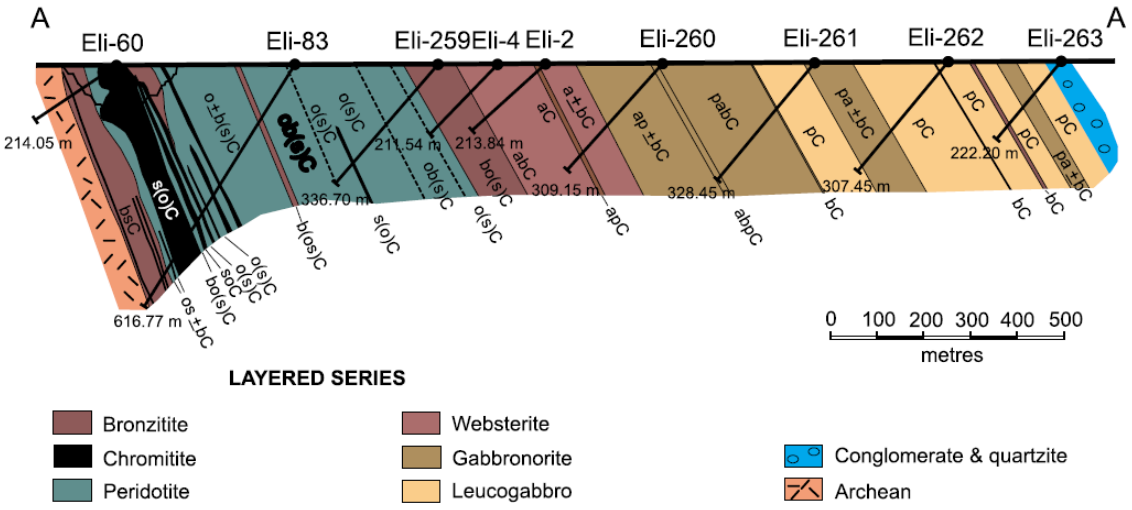

Figure 5. Profile of the Kemi layered intrusion at the Elijärvi ore lens. Location of the profile shown in Figure 4. Abbreviations in Table 2 (from Alapieti and Huhtelin, 2005). Published with permission from Elsevier.

The basal sequence of the Kemi intrusion (10 to 40 m thickness) at the contact with the underlying Archean basement is characterized by a mylonitic talc-chlorite-carbonate

schist and occasional talc-carbonate rock. Euhedral chromite phenocrysts (0.5 mm diameter) are the only primary mineral preserved in this rock and accounts for 15% vol (Alapieti et al., 1989, Alapieti and Huhtelin, 2005; Huhtelin, 2015). Discontinuous layers of gabbroic composition can also be found in mylonites. Grain size of the gabbro increases further away from the contact with the basement. Where these gabbros are thicker and more continuous, an overlying layer of pyroxenite can be recognized on the top of them (Huhtelin, 2015). The above mentioned features suggest the existence of a marginal series which was eroded during the magmatic stage (Alapieti et al., 1989; Huhtelin, 2015).

Above the basal sequence there is a layer of about 40 – 100m of altered rocks. The lower part is composed of cumulates of bronzite – chromite. Xenoliths of the underlying basement are common in this layer. The upper part consists of cumulate of olivine – chromite ± bronzite with interlayers of chromitite with 0.5 – 1.5m thickness (Alapieti et al., 1989, Alapieti and Huhtelin, 2005). Chromitite interlayers and disseminated chromite (roundish lumps) can also be recognized in the upper layer. This layer is overlain by the main chromitite zone.

The main chromitite layer has an average thickness of around 40 m in the mining area. At the center of the intrusion it forms two layers separated by a Si-rich layer. The cumulate minerals are chromite-olivine with intercumulate poikilitic bronzite ± augite. The lower parts are commonly non-layered and disseminated (Alapieti et al., 1989, Alapieti and Huhtelin, 2005). The relation of chromite – olivine is higher in the upper parts. However, a thin layer of cumulate olivine ("spotted type" in mine nomenclature) is also encountered in the upper parts (Huhtelin, 2015). Bronzite becomes the main cumulate mineral in the silicate-rich part, characterized by large bronzite crystals surrounded by chromite.

A 550m thick layer of peridotite cumulate (Fig. 6a) rests on the top of the main chromitite layer. This layer is characterized by olivine – chromite ± bronzite as the cumulate minerals. Interlayers of chromitite and pyroxenite are also recognized. The sequence has 15 layers of chromitite of varying thickness (5cm – 2.5m), with the uppermost one being located 370m above the main chromitite unit. The pyroxenite layers are found in the lower parts of the sequence and have varying thickness of 10 – 30m. The uppermost pyroxenite shows rhythmic layering with intervals of olivine ± chromite and olivine – bronzite ±

chromite cumulates with augite as the main intercumulate mineral. 700m above the basal contact of the intrusion bronzite (Fig. 6b) becomes the main cumulate mineral, with minor chromite and olivine. After 100m above, augite becomes the dominant cumulate mineral (Fig. 6c), and chromite and olivine disappear (Alapieti et al., 1989, Alapieti and Huhtelin, 2005).

1000m above the basal contact, plagioclase becomes the main cumulate mineral with minor bronzite and augite (Fig. 6d). This layer extends for about 800 m until the contact with the hanging wall. In the upper section there is little bronzite and augite found as the intercumulate mineral (Table 2; Alapieti et al., 1989, Alapieti and Huhtelin, 2005).

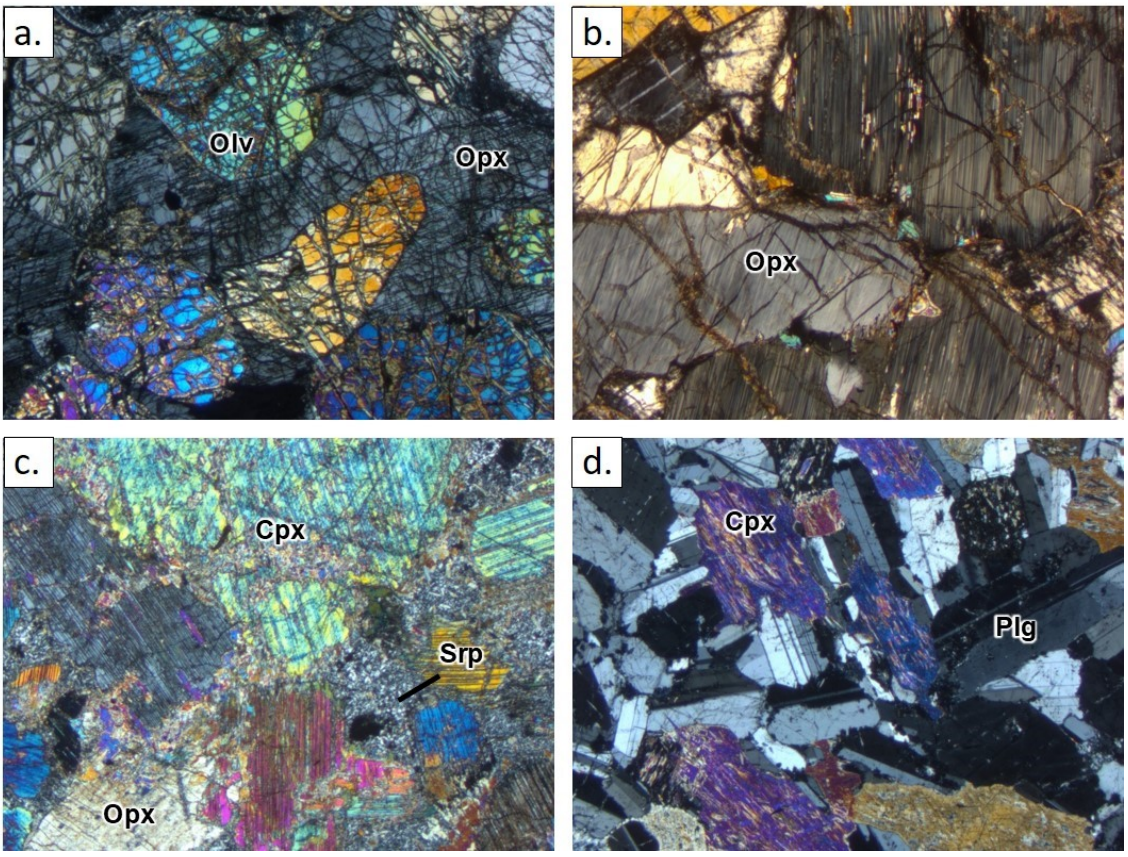

Figure 6. Photomicrograph in crossed polarized light of different layers from Kemi intrusion. (a) Peridotite, sample ELI-259-199.70. (b) Bronzite, sample ELI-259-125.80. (c) Websterite, sample ELI-2-108.10. (d) Gabbronorite, sample ELI-261-328,10. Width of photograph = 4.26 mm. Cpx = clinopyroxene, Olv = olivine, Opx = orthopyroxene, Plg = plagioclase, Srp = serpentine.

Table 2. Nomenclature used in the cross section (Fig. 5; from Alapieti and Huhtelin, 2005). Published with permission from Elsevier

Conventional rock name	Cumulus mineral assemblage	Cumulate abbreviation
Peridotite	Olivine ± bronzite ± chrome spinel	o ± b ± sC
Chromitite	Chrome spinel (± minor olivine)	s(o)C
Bronzitite and olivine bronzitite	Bronzite-olivine (± minor chrome spinel)	bo(s)C
Websterite and diallagite	Augite ± bronzite	a ± bC
Gabbronorite and gabbro	Plagioclase-augite ± bronzite	pa ± bC
Leucogabbro and anorthosite	Plagioclase	pC

The Kemi intrusion is also intersected by three types of dikes (Alapieti et al., 1989). The first type is albite diabases of varying thickness (few centimeters to 20 m) with ophitic cores and decreasing grainsize to the margins which are altered to chlorite. Chlorite has totally altered smaller dikes of this type. The second type is albitite dikes of 1 to 10m thickness, and the third type is granite dikes in the basal section of the intrusion with compositions similar to that of the granitic basement. Grönholm (1994) also mentioned the occurrence of scarce dikes of quartz, quartz keratophyre (metamorphosed felsic volcanic rock) and carbonate-feldspar (with gold).

The lower and upper parts of the Kemi intrusion have been affected by extensive alterations being stronger over the gangue minerals (Alapieti et al., 1989, Alapieti and Huhtelin, 2005). Alteration on chromite has affected the edges and cracks of the grains, leaving the cores still intact. The content of Al and Mg drops sharply to the edges, opposite of Fe and Ni which in turn increase (Alapieti and Huhtelin, 2005). It is also recognized in some of those grains the development of magnetite rims and corrosion produced by serpentinization. Furthermore, chromite grains contain inclusions of altered olivine (talc-serpentine; Alapieti et al., 1989). Alteration of the gangue in the lower part of the intrusion is widespread from the bottom up to the layers immediately above the main chromitite unit (Alapieti et al., 1989, Alapieti and Huhtelin, 2005). Cumulate sequences have been altered in different proportions to serpentine, talc, carbonate,

amphibole, chlorite, magnetite and phlogopite. Veins filled with carbonate and talc are also widely recognized.

Grönholm (1994) carried out a detailed study about the altered rocks. The study was mainly focused on the peridotites and pyroxenites. The peridotites studied in this work are either slightly fresh or heavily altered. In the case of pyroxenite, fresh samples are also recognized and more common. The most abundant mineral in all the peridotites is serpentine, followed by varying proportions of chlorite, amphibole, magnetite and carbonate. Pyroxenites are either fresh or altered to abundant proportions of amphibole or talc, with different fractions of chlorite, serpentine, magnetite and carbonate.

3 METHODOLOGY

The material of study for this work were 49 thin sections from Grönholm (1994) work. Each of the thin sections was studied for petrographic analyses under an "Axioplan 2" (Zeiss) microscope, coupled with an "Axiocam 105 color" camera. Samples were checked rigorously in order to describe mineral textures and alteration features. Representative photographs of these characteristics were taken.

From the bulk of samples, 23 thin sections were chosen for microprobe analyses, taking into account the sample's lithology, distribution, depth and minerals. The thin sections were carbon coated and later studied in a JEOL JXA-8200 electron microprobe in the facilities of the Center of Microscopy and Nanotechnology at the University of Oulu. Operating conditions were of 15 kV of accelerating voltage, 10 um of probe diameter, and beam current of 15.58 nA.

4 PETROGRAPHY

In this section a detailed description of the thin sections was done taking into special consideration the different types of hydrothermal alterations and the relations between each of them. Abbreviation of the modal composition of the rocks can be found in Appendix 1 and the modal compositions in Appendix 2 to 9. As mentioned above, thin sections for the petrographic description Grönholm (1994) samples were used. All the studied samples are either peridotites or pyroxenites. Distinction between peridotites and

pyroxenites was done following Streckeisen classification of ultramafic igneous rocks in which rocks containing more than 40% olivine are considered peridotites and rocks beneath that limit are considered pyroxenites (Le Maitre et al., 2002).

As expected in layered intrusions, rocks from the Kemi intrusion show cumulate textures. Peridotites and pyroxenites are mostly of the orthocumulates (Fig. 7). In peridotites, euhedral olivine grains are surrounded by anhedral orthopyroxene and clinopyroxene. In pyroxenites, orthopyroxene is the dominant cumulate mineral (with occasional presence of olivine) and is surrounded by anhedral clinopyroxene.

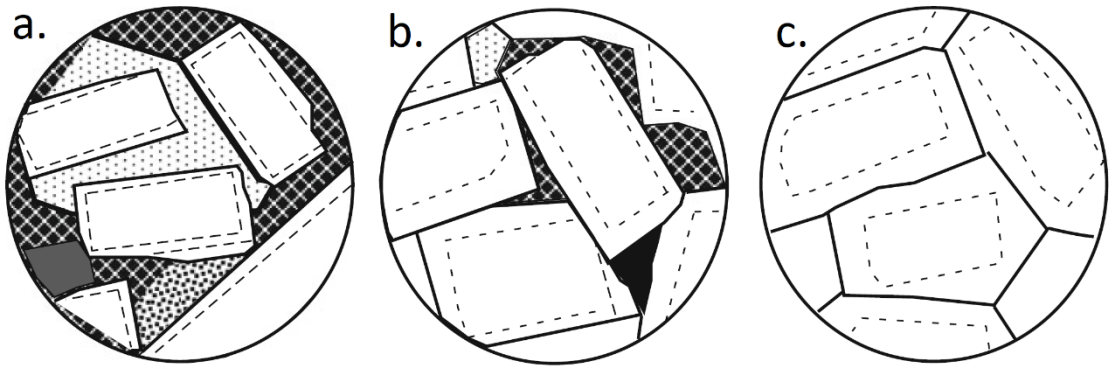

Figure 7. Sketch of cumulate textures in layered intrusions. (a) Orthocumulate texture. (b) Mesocumulate texture. (c) Adcumulate texture. Dashed lines indicate the original borders of the cumulate crystals. From Sen (2014).

The main focus in Grönholm (1994) was the feasibility of using Kemi mine gangue as rock aggregates. For the present work the classification of Grönholm (1994) was used since it takes into special consideration of the host rocks of the Kemi ore. Average modal composition of the lithologies in Grönholm (1994) are shown in Fig. 8. Criteria of classification for the studied lithologies can be found in table 3, abbreviation of the mineral names used in this work can be found in table 4. Peridotites are grouped in; cumulate peridotites, chlorite peridotites, amphibole peridotites, serpentine peridotites and pyroxene peridotites. Petrographic description of the peridotites is presented into two groups; cumulate peridotites and “altered peridotites”. Cumulate peridotites are the freshest samples of this study (~76% altered). Altered peridotites are formed by the remaining chlorite, serpentine, amphibole and pyroxene peridotites. These rocks are altered from 95 to 100%. Even though the peridotites are classified in different groups, they all show a similar alteration pattern varying only in the intensity of alteration and

mineral volumetric percentages.

Pyroxenites in the area of this study are bronzites, websterites and diallagites (Alapieti et al 1989). Pyroxenite in this study only include altered bronzites – olivine bronzites (amphibole pyroxenites and talc pyroxenites). Description for both pyroxenite groups is presented in the "pyroxenites" section. A similar approach is carried for the description of the pyroxenites, where amphibole pyroxenites and talc pyroxenites share vary similar characteristics.

Samples of this study containing more than 70% serpentine are classified as serpentinites (Grönholm, 1994). From the five serpentinite thin sections, three are considered peridotite-derived, only one is considered dunite-derived and one has all of its primary features obliterated by alteration (protolith unidentified). Since each serpentinite sample has a different alteration texture, description is conducted for each thin section.
Only two thin sections of chromitites were described in this work (ELI-436-112.00 and ELI-453-42.10).

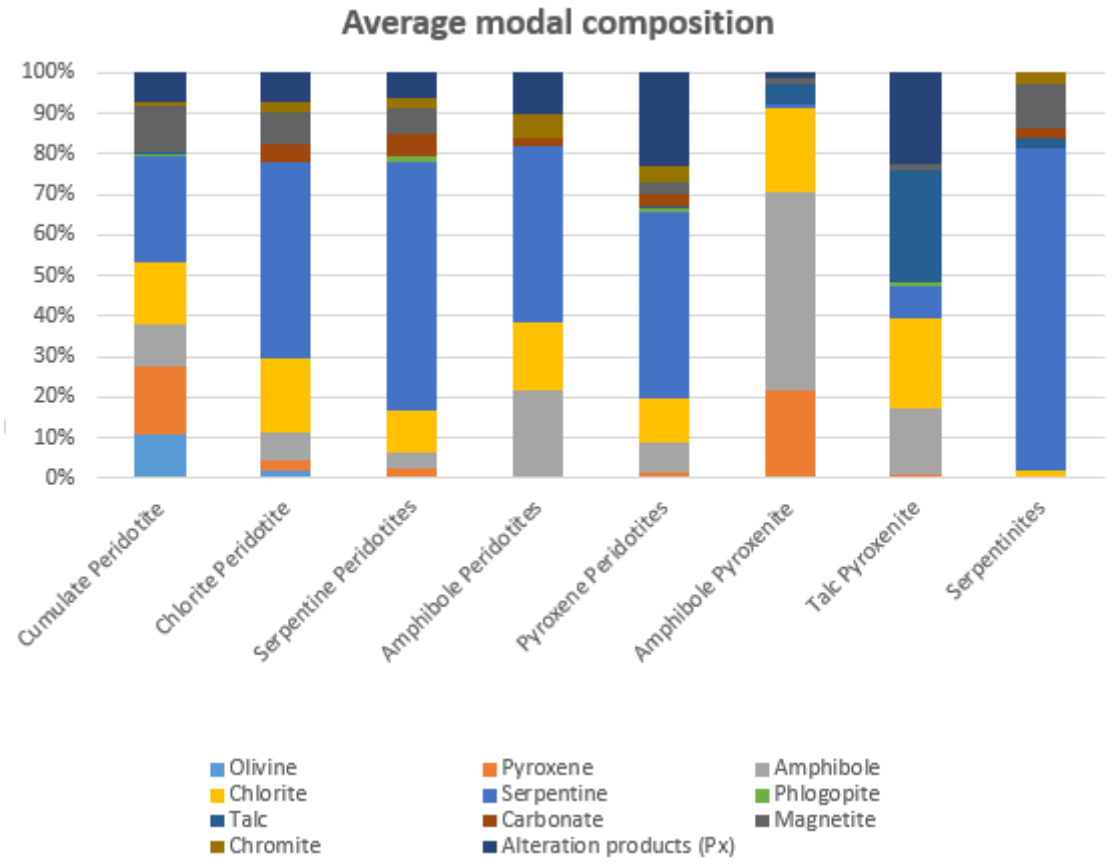

Figure 8. Average modal composition of the lithologies in Grönholm (1994).

Table 3. Criteria for classification of the ultramafic rocks in Grönholm (1994).

Lithology	Subgroup	Criteria
Metaperidotites	Cumulate peridotites	Least altered peridotites, easily recognized primary features and abundant relicts.
	Chlorite peridotites	Abundance of chlorite altered intercumulus from 14.9% to 22.6%.
	Serpentine peridotites	Most altered peridotites, containing from 56% to 68% serpentine.
	Amphibole peridotites	Similar to chlorite peridotite but with higher abundance of amphibole (14.8 - 28.4%).
	Pyroxene peridotites	Abundance of alteration products of pyroxene varying from 18% to 40%
Pyroxenites	Amphibole pyroxenite	Pyroxenites with a marked abundance of amphibole (29.4% - 76.6%).
	Talc pyroxenite	Pyroxenites with plentiful talc alteration (13.3% - 18.8%).
Serpentinites (71.3% - 90.2% serpentine)	Derived from peridotite	Orthocumulus texture.
	Derived from dunite	Adcumulus texture and abundant olivine alteration products.

Table 4. Abbreviations of the mineral names used in this work.

Name	Abbreviation
Alteration products (px)	Alt(px)
Amphibole	Amp
Apatite	Ap
Carbonate	Crb
Chlorite	Chl
Chromite	Chr
Clinopyroxene	Cpx
Magnetite	Mt
Olivine	Olv
Orthopyroxene	Opx
Phlogopite	Phl
Serpentine	Srp
Talc	Tlc

4.1 Cumulate peridotites

These rocks have extensive hydrothermal alteration, nonetheless relicts of primary minerals and textures are preserved, unlike the other peridotites.

Olivine crystals are intensely fractured, forming an array of clustered fragments with a

mesh-ribbon texture (Fig. 9a - d). These fragments are either relict olivine, serpentine, or chlorite altered hourglass serpentine. Ribbons between the fragments show abnormal green color in both crossed polarized light (CPL) and plane polarized light (PPL) as well as white color in both PPL and CPL, corresponding to Fe-bearing serpentine. The fractures that host the ribbons are protracted in the rock. However, ribbons mainly occur in olivine grains and in lower proportion to almost absent in the pyroxenes. A common feature in olivine crystals is the deposition of magnetite over the ribbons, especially in areas near the center of the grain. In the rim of the grain, olivine crystals are altered to flakes and needles (Fig. 9a and e) which have interpenetrating textures and are formed of amphibole and serpentine, being more abundant where the olivine is in contact with the chlorite-altered intercumulate. Amphibole is also found in later veins crosscutting olivine crystals and the ribbons inside them.

Most of the intercumulate pyroxene has been pervasively altered leaving few relict occurrences. Relict orthopyroxenes are fractured but not as much as olivine grains. Orthopyroxenes are commonly altered to bastite in different proportions, with some grains completely altered (Fig. 9a). Veins of fine grained amphibole are more common in orthopyroxenes but amphibole rims are scarce. Observed relict clinopyroxene remains mostly unaltered (Fig. 9c), it is crosscut by fractures and amphibole veins, and it's occasionally altered to amphibole flakes in the rims when in contact with the chlorite-altered intercumulate.

The altered intercumulate minerals are difficult to describe due to extensive hydrothermal alteration and fine grained nature. Two types of altered intercumulate were recognized (100% replacement for alteration assemblage): the chlorite-altered intercumulate (Fig. 9a and e) and the "alteration products (px)". The latter refers to the alteration assemblages of intercumulate pyroxene (hence the "px") following Grönholm (1994) nomenclature, explained in the lines bellow.

The chlorite-altered intercumulate is colorless to bluish-greenish in PPL and gray, greenish-bluish (abnormal colors) to isotropic in CPL. It is formed by fine grained disseminated flakes (greenish-gray-white), flakes in interpenetrating aggregates (greenish-blue-gray) and discontinuous ribbons (gray-white), contained by an isotropic matrix. The geometry of the above mentioned minerals is characteristic of serpentine

aggregates (Wicks and Whittaker, 1977), nonetheless, as pointed by microprobe studies from this work and as mentioned in Grönholm (1994) most of the mineral is composed of chlorite.

The “alteration products (px)” is present throughout all of the peridotites. The alteration products (px) are characterized by very fine grained aggregates of different minerals in varying proportions, hard to distinguish by the use of the optical microscope only (Grönholm, 1994). Therefore the specific minerals were not taken into account for volumetric percentages but counted as a whole group. Alteration products (px) in the cumulate peridotites is scarce compared to other peridotites, which is observed mostly as aggregates of flaky amphibole and serpentine.

Phlogopite is also recognized in the cumulate peridotites as an intercumulate mineral (Figs. 9e and f). Phlogopite occurs as tabular anhedral aggregates, always at a close distance or surrounding chromite grains.

Chromite in the optical microscope seems to be unaltered, only affected by minor fracturing (Figs. 9e and f).

Later serpentine veins are observed crosscutting the sample, finding in sample ELI-67-9.3-9.4 one also crosscutting an amphibole vein.

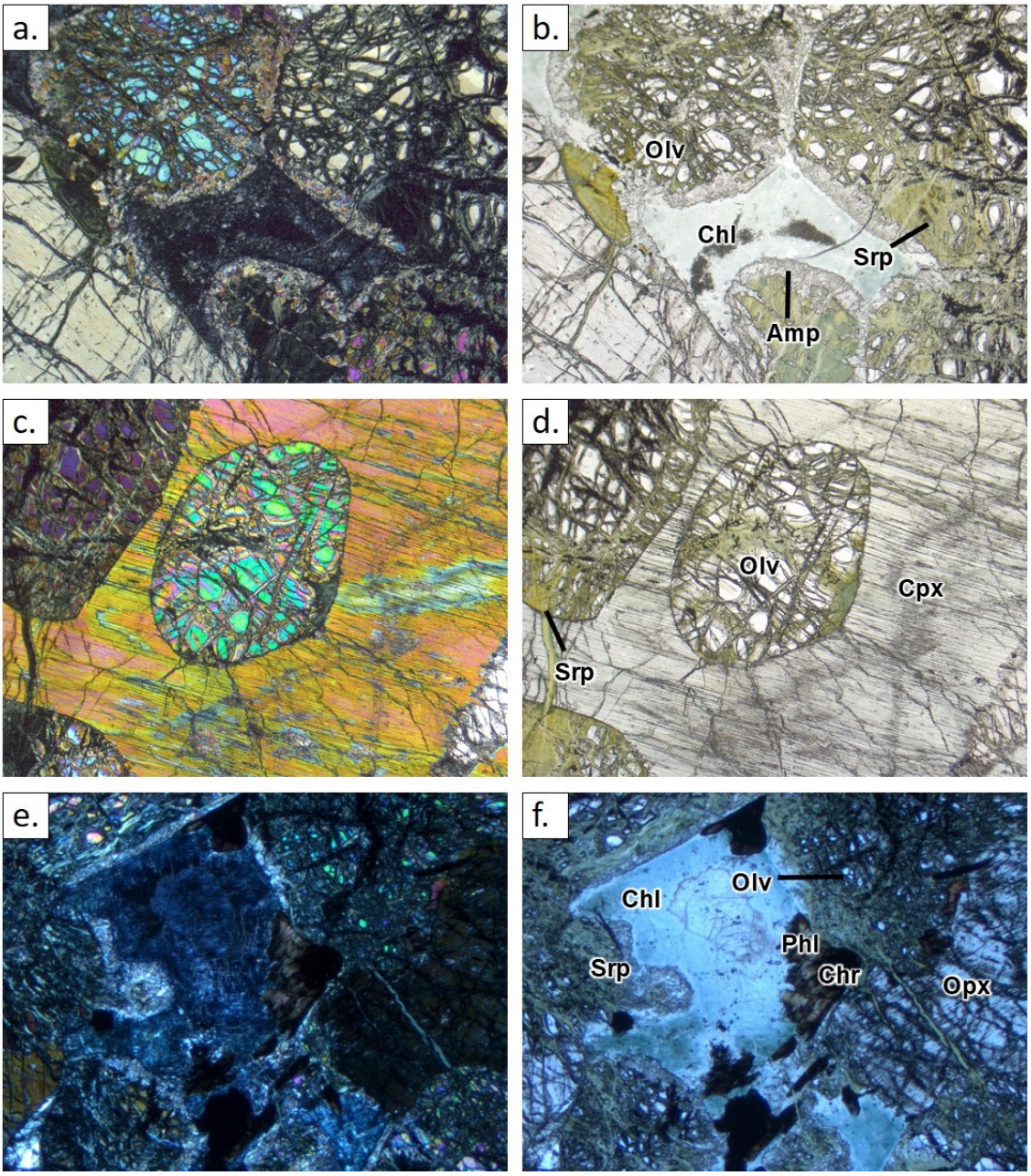

Figure 9. Cumulate peridotites, sample ELI-67-9.30-9.40. a.) CPL, serpentine partly-altered olivine (mesh-rim texture) with amphibole-altered (flakes) rims. Altered orthopyroxene is observed in the bottom left corner, chlorite intercumulate in the middle. Ribbons in olivine are overprinted by chlorite and magnetite. b.) Same picture in PPL. c.) CPL, poikilitic texture of clinopyroxene and olivine. Fractures crosscut both crystals but ribbons are only formed in olivine. Ribbons are masked by magnetite. d.) Same picture in PPL. e.) CPL, phlogopite surrounding chromite (middle of the picture). Small white serpentine flakes are disseminated in the chlorite intercumulate. Altered pyroxene and olivine are observed in all borders of the picture. f.) Same picture in PPL. Widths of the photos a – d = 1.6mm, photos e – f = 3.6mm.

4.2 Altered peridotites

Relict minerals are rarely observed in altered peridotites, as these lithologies are

pervasively altered to almost 100%. Identification of primary cumulate texture is possible since the alteration minerals usually preserve the primary shape of grains, nonetheless alteration in some cases obliterates those features (e.g. when both olivine and pyroxene are altered to serpentine) being only possible to distinguish between the cumulate crystals from the intercumulate due to precipitations of magnetite in the rims.

Olivine relicts is only recognized in a few samples with less than 6.5%. In altered peridotites olivine is almost entirely replaced by different types of serpentine. Unlike cumulate peridotites, aggregates of serpentine flakes and fibrous aggregates are the dominant types of serpentine (Figs. 10a - f and 11a - f), followed by occasional occurrences of partially recrystallized serpentine ribbons and mesh cores. Serpentine flakes occur as either interpenetrating textures throughout the original olivine grain (Fig. 10c – d) or preserving resemblance to the previous mesh-ribbon texture (where some ribbons and mesh cores can still be recognized). In mesh-ribbon textures, the flakes usually follow the geometry of the mesh centers and some still preserve the hourglass centers geometry (Fig. 10a - b). Occasionally, mesh cores (obliterated by flake recrystallization) are rimmed by magnetite and can be easily identified. Flakes also grow perpendicular to the former subparallel ribbons (usually two different directions; Fig. 11a - b), giving the sample a foliated appearance.

Frequently, serpentine-altered olivine crystals are rimmed by flaky and acicular amphibole (Fig. 11a – b). Alteration is stronger when in contact with chlorite alteration intercumulate. The amphibole flakes are bigger in some of the samples when alteration degree is stronger, with amphibole masking the serpentine-recrystallized mesh centers. When carbonate is present in the sample, it usually forms a second rim around the amphibole flakes and/or disseminated random aggregates within the original olivine crystal grain. Amphibole flakes are sporadically overprinted by talc alteration, showing higher order interference colors.

Intercumulate pyroxene in the samples are altered to a wide range of minerals. Distinction between the alteration minerals of clinopyroxene and orthopyroxene is challenging and the occurrence of relict pyroxenes is scarce, only few clinopyroxene crystals were identified. This is probably because clinopyroxenes are more resistant to serpentine alteration (Wicks and Whittaker, 1977). Serpentine alteration over pyroxene is almost

ubiquitous, occurring in different proportions (~2% to 100%) either as bastite (patchy, pervasive or along cleavage; featureless and/or fibrous) or serpentine flakes.

Scarce relict clinopyroxene is only partly altered and is easily distinguished from other rock forming minerals (Fig. 10e – f). Serpentine alteration (flakes and bastite) in relict clinopyroxene proceeds along fractures and cleavage.

Amphibole is also a common alteration product in pyroxenes. Intergrowths of serpentine and amphibole in pyroxene occur as aggregates of flakes (Fig. 11c – d). The parallel subhedral elongated amphiboles are with (or without) a matrix of serpentine and intergrowths of bastite (replacement along cleavage). Pyroxene grains are occasionally rimmed by amphibole (flakes). Amphibole in PPL is either colourless or brownish. Under CPL, the colors are brownish to second order colors. Only in one sample, amphibole-serpentine-magnetite altered pyroxene intercumulate exhibits clean (devoid of magnetite speckles) amphibole rims growing inwards serpentine-altered olivine grains (opposed to the usual rims developed towards the intercumulate grains; Fig. 10c - d).

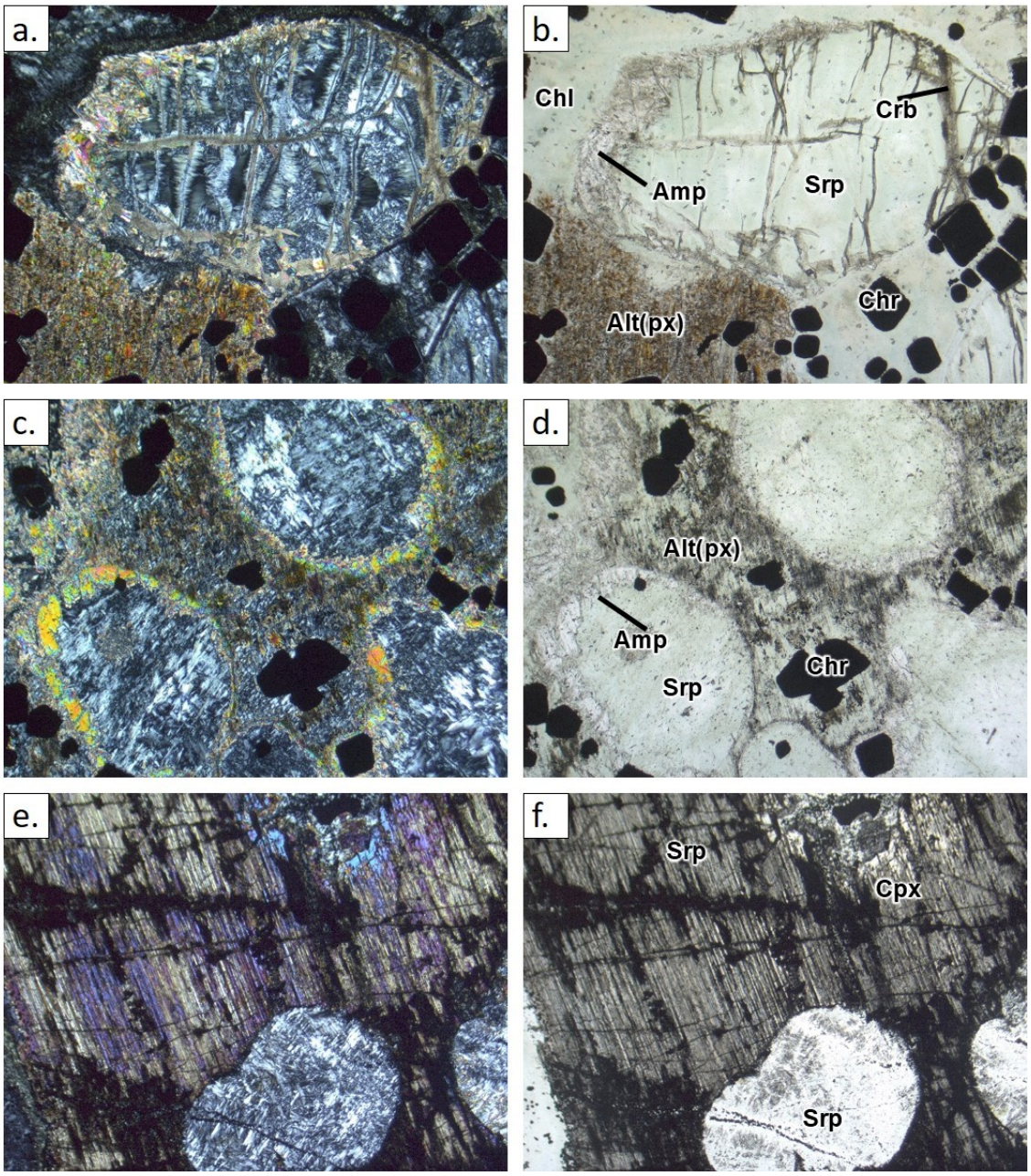

Figure 10. Samples belong to the pyroxene peridotites of the altered peridotites. a.) Sample ELI-670-43.50 in CPL. Serpentine altered grain with hourglass texture, overprinted by fibrous serpentine. The same grain is rimmed by amphibole flakes and has carbonate replacement along the fractures. A grain of amphibole-altered pyroxene can be observed in the left bottom corner. Amphibole is slightly pleochroic and is partly mantled by magnetite. Amphibole interference colors increase due to talc alteration. b.) Sample Eli-670-43.50 in PPL. c.) Sample ELI-674-77.40 in CPL. "Alteration products (px)" surrounding serpentine-altered olivine grain. Amphibole and serpentine (fibrous and flaky aggregates) can be easily recognized in the alteration products (px). Amphibole rims grow inwards the former olivine grain. d.) Sample ELI-674-77.40 in PPL. e.) Sample ELI-672-5.7 in CPL. Clinopyroxene altered to fibrous bastite and magnetite along cleavage and fractures. f.) Sample ELI-672-5.7 in PPL. Width of the photos = 1.6 mm

Occasionally, chlorite overprints bastite altered pyroxenes.

Phlogopite is observed with brownish colors in both CPL and PPL, often pleochroic and masked by magnetite (Fig. 11a – b). Phlogopite is also frequently identified in the surroundings of chromite grains. Phlogopite content is usually less than 1%, nonetheless it reaches up to 8% in one sample (ELI-47-20.57).

"Alteration products (px)" occurs as a complex aggregate of very fine gained alteration minerals. Contact between the alteration products (px) and serpentine is rarely sharp, mostly developing intergrown serpentine flakes or alteration rims (Figs. 11a, b, e and f). Most common alteration minerals of the alteration products (px) are amphibole, magnetite and serpentine, followed by carbonate, talc, chlorite and phlogopite. These minerals are not exclusive to the alteration products (px), when present they are also identified throughout the sample (e.g. amphibole rims around former olivine grains, aggregates and veins of carbonate).

The chlorite-altered intercumulate occurs in a similar fashion to the Cumulate Peridotites (Figs. 10a – b and 11c – d), but opposed to them chlorite-altered intercumulate abundances higher due to more intensive hydrothermal alteration. The above-mentioned alteration rims (amphibole, carbonate, talc) are generally developed when in contact with chlorite-altered intercumulate. Disseminated crystals and aggregates of carbonate and talc are also identified in the chlorite-altered intercumulate.

Magnetite is another alteration product of pyroxene, occurring in different proportions. It's observed usually as speckles all over the pyroxene crystal (Figs. 10a – d; 11a – b and 11e - f), forming along cleavage and/or fractures (Fig. 10e – f) and masking the pyroxene crystals. Based on magnetite alteration and the speckled appearance, as well as precipitation on the rims of the crystals, it is easy to differentiate between former olivine and pyroxene grains.

Carbonate is observed as rims surrounding former olivine and pyroxene crystals (Fig. 11c – d), usually as a second rim with an inner rim of amphibole and as precipitations along the former serpentine ribbons (Fig. 10a – b). Carbonate is also found in veins (Fig. 11e) as well as disseminated aggregates within serpentine-altered olivine, as a replacement mineral in the "alteration products (px)" (Fig. 11a – b) and disseminations in chlorite-

altered intercumulate.

Talc occurs as an alteration assemblage in the “alteration products (px)” (Fig. 11a – b), rarely being very abundant. Talc is observed as aggregates of flakes after pyroxene. Talc also seems to be masking amphibole, evidenced by the increase interference colors of amphibole almost to the third order colors.

Chromite in the peridotites are commonly fractured and occasionally corroded. Borders of chromite grains are usually recrystallized and its surroundings slightly devoid of opaques (when contained by magnetite-rich altered pyroxene; Fig. 11e).

Apatite is identified as a cumulate accessory mineral, being only recognized in one sample (ELI-670-15.50) as an elongated prismatic crystal (Fig. 11a – b) in contact with phlogopite and alteration products (px).

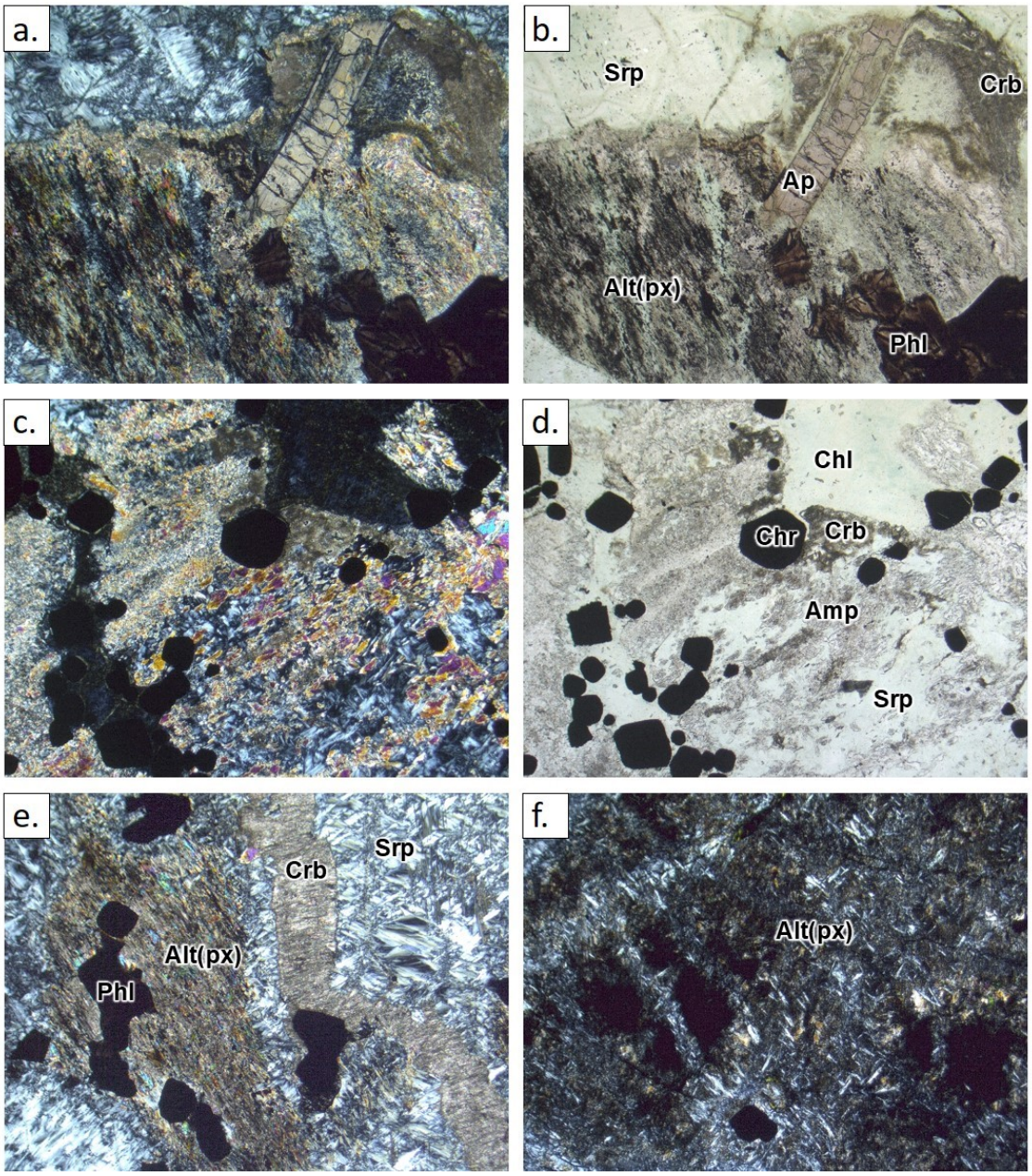

Figure 11. Altered peridotites. a.) Sample ELI-670-15.50 of the serpentine peridotites in CPL. Alteration products (px) with aggregates of phlogopite (lower right corner). A prismatic grain of apatite can be identified in the middle of the upper half of the picture. b.) Sample ELI-670-15.50 in PPL. c.) Sample ELI-674-77.40 of the pyroxene peridotites in CPL. Pyroxene grain partly rimmed by carbonate (near the biggest chromite grain in the picture) and altered to serpentine and amphibole flakes. d.) Sample ELI-674-77.40 in PPL. e.) Sample R25.5-65.75 of the chlorite peridotites in CPL. Alteration products (px) surrounding phlogopite and chromite with serpentine flakes aggregates and a carbonate vein. f.) Sample ELI-672-5.7 of the pyroxene peridotites in CPL. Very fined grained assemblage of the alteration products (px). Serpentine flakes (White) and magnetite mantling can be easily recognized. Width of the photos = 1.6 mm.

4.3 Pyroxenites

Cumulate crystals are usually subhedral prismatic (short) crystals with celluloid shapes

(after Hibbard, 1995). Alteration over pyroxene in most of the crystals occurred along cleavage, giving a foliated appearance. Pyroxene grains are mostly altered to amphibole, nonetheless this alteration occurs with different characteristics.

Pyroxene grains are altered along cleavage in parallel-subparallel relation, producing subhedral-euhedral elongated prismatic amphibole needles. The amphibole needles grow perpendicular to crosscutting fractures along pyroxene grains (Fig. 12a). Different proportions of matrix are found between amphibole needles. This matrix can be serpentine, opaques, amphibole flakes, talc and/or carbonate. Aggregates of amphibole needles are frequently rimmed by abundant amphibole flakes (Fig. 12b).

Pyroxene grains are also altered to subparallel - randomly oriented amphibole flakes (Fig. 12c), occasionally in flame textures. The matrix of this aggregates is either serpentine, chlorite or finer grained amphibole flakes.

Alteration to amphibole in some grains seems to be succeeding bastite alteration. These grains show intergrowths of parallel and oriented grains of amphibole and bastite, giving the appearance of a chessboard texture (Fig. 12d – f).

Subrounded amphibole-altered primary grains are also observed. Alteration occurs as unoriented flakes of amphibole, either as rims (surrounding the serpentine-altered grain) or as a pervasive alteration throughout the crystal (Fig. 12c). This alteration is very similar to the amphibole alteration of olivines in the peridotites, therefore these grains are considered to be altered olivines.

When olivine is present, it is enveloped by pyroxene. In some of the contacts between altered pyroxene and altered olivine grains, bastite and amphibole rims (growing inwards the cumulate olivine) are observed with a neat and opaque-devoid appearance (contrary to the opaque-rich pyroxene). When altered to amphibole, both rims and pyroxene appear to be a same crystal, with equal extinction and interference colors (Fig. 13a).

Observed chlorite intercumulate in the pyroxenites share similar features with the chlorite intercumulate in peridotites. The contact with the other mineral phases lacks sharp borders, occurring usually as intergrowths of alteration minerals. Alteration rims also tend

to be more developed when in contact with chlorite intercumulate. In pyroxenites, greenish flake aggregates (CPL) are more common and normally bigger (Fig. 13b).

Opaque minerals (mainly magnetite) in the sample occur as disseminations in the matrix, forming rims on the grains (both alteration and primary grains), along cleavage or random disseminations giving a speckled appearance. Chromite is almost absent in the pyroxenite samples

Carbonate is observed as very fine-grained aggregates, occurring randomly, either at crystal borders, matrix, or altering the core of amphibole-rimmed grains.

Phlogopite is present on the samples as intercumulate mineral, being more abundant in the talc pyroxenites. Phlogopite appears as pleochroic aggregates of brownish colors in both CPL and PPL, occasionally masked by magnetite.

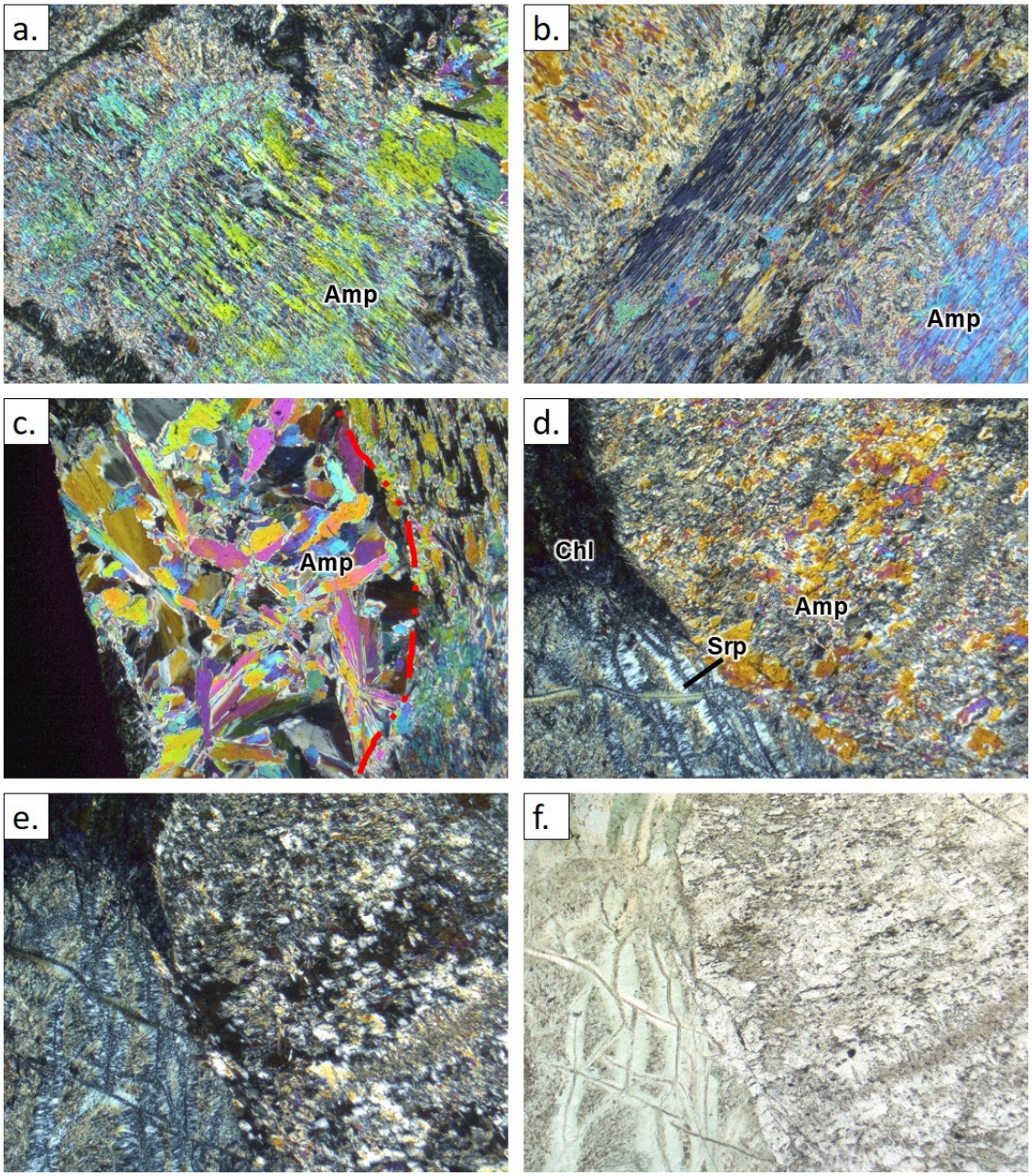

Figure 12. Amphibole pyroxenites. a.) Sample ELI-674-73.0 in CPL. b.) Sample ELI-672-34.00 in CPL. a.) and b.) show alteration of pyroxene by prismatic/needle shaped amphibole. In a.) some of the crystals can be seen growing from fractures of SW-NE direction (of the photo). In b.) the coarser amphibole is surrounded by finer grained amphibole. c.) Sample ELI-672-45.60 in CPL. Olivine grained replaced by randomly oriented amphibole flakes (highlighted with red dashed-line). d.) Sample ELI-670-52.50 in CPL. Bastite and amphibole altered pyroxene on the right-hand side of the photo. e.) Same association in sample ELI-670-52.50 (CPL). The plate is slightly rotated. Bastite and amphibole aggregates display a "chessboard" texture. f.) Same association in PPL. Width of the photos = 1.6 mm.

Talc pyroxenites are fairly similar to amphibole pyroxenites, suggesting similar alteration processes. The differences lie in a marked higher abundance of very fine-grained aggregates (Fig. 13b) and the lack of "chessboard" aggregates of amphibole and bastite.

Amphibole alteration occur in a similar fashion in both groups, however, amphibole flakes and needles tend to be smaller, the matrix between coarser alteration grains is notoriously more abundant and its main mineral is talc.

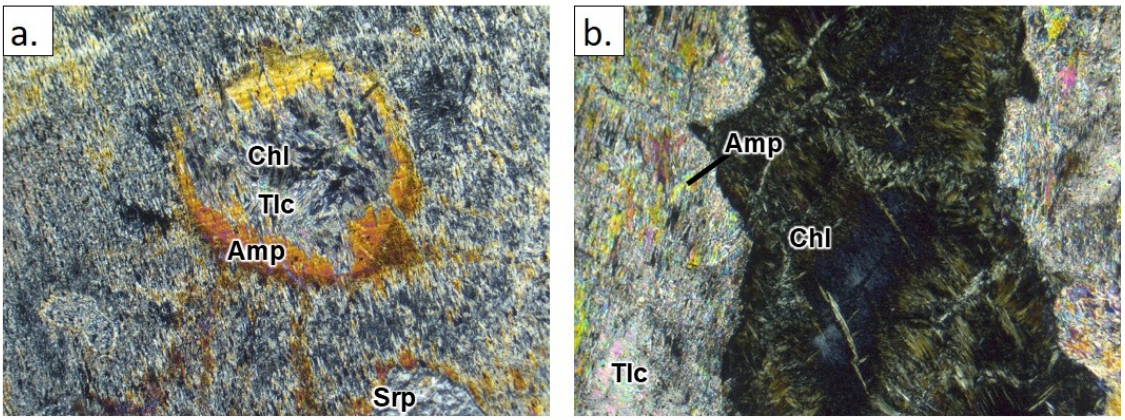

Figure 13. Talc pyroxenites. a.) Sample R25-57 in CPL. Poikilitic texture of olivine and pyroxene. Both minerals are altered to talc, serpentine, chlorite and amphibole, they can only be differentiated thanks to amphibole rims growing inwards the olivine grain. b.) Sample R25-3-27 in CPL. Amphibole and talc altered pyroxene in the left-hand and right-hand border of the picture, chlorite intercumulate in the middle. Amphibole (needles) altered pyroxene has rims and matrix of fine grained talc aggregates. Chlorite intercumulate has anomalous greenish and bluish colors. Width of the photos = 1.6 mm.

4.4 Serpentinites

A common feature in all of the serpentinites is the corrosion of chromite grains as well as alteration of chromite along their margins. Peridotite-derived serpentinite still preserve features of the orthocumulate textures, relatively easy to recognize due to magnetite alteration and differences in grainsize and texture (e.g. differences in grainsizes between intercumulate and cumulate minerals in sample ELI-512-34.80, explained in the lines bellow; Fig. 14a – b).

The main recognizable features of sample ELI-51-140.39 are protracted mesh-rim textures, which are overprinted by serpentine-flake alteration. These domains are enveloped by the scarce intercumulate which is altered to finer grained aggregates of interpenetrating serpentine, isotropic serpentine and chlorite.

Sample ELI-731-147.45 is a dunite-derived peridotite. The entirety of the sample is formed by aggregates of serpentine in a mesh-rim texture (Fig. 14c – d). Magnetite occurs

in the border of the former olivine grains as well as over the ribbons.

Distinction between cumulate and intercumulate phases is more complicated in sample ELI-512-34.80, the only indication are the differences in the grain sizes. Intercumulate tend to be formed by fine grained aggregates of flaky serpentine while cumulate minerals are formed by coarser flakes of serpentine. A cumulate crystal is also observed in one of the corners of the section with mesh-rim textures overprinted by serpentine flakes. The sample is also cut by banded serpentine, magnetite and carbonate veins. Deformation in this thin section is evidenced by the development of thrusts and folds in the aforementioned veins (Fig. 14e – f).

Intercumulate grains are difficult to recognize in sample ELI-550-38.55, present as fine grained aggregates of serpentine with interlocking and interpenetrating textures. Cumulate grains exhibit a mesh-rim texture, overprinted by flaky serpentine. Carbonate is also observed in the sample as disseminated very fine-grained aggregates.

Sample ELI-SP-2 is composed by aggregates of serpentine flakes with small amounts of carbonate and talc aggregates. Alteration has obliterated the primary features, making it difficult to determine a protolith.

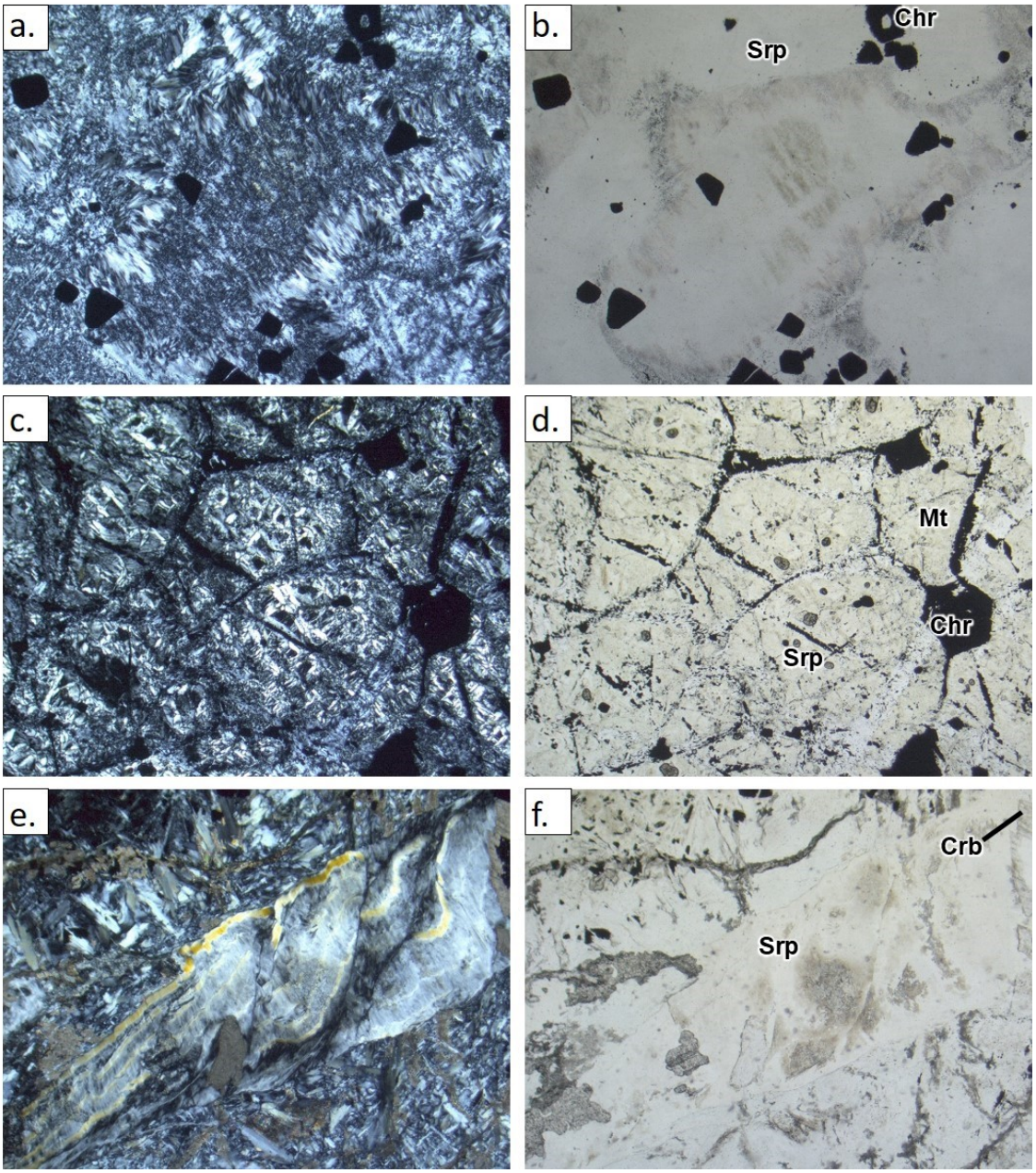

Figure 14. . Serpentinites. a.) Sample ELI-556-38-55 in CPL. Fine-grained aggregates of serpentine (middle of the picture) surrounded by coarser, flaky serpentine. b.) Same association in PPL. Besides grain size, disseminated magnetite helps differentiating between cumulate and intercumulate minerals. c.) Sample ELI-731-147.45 (dunite derived) in CPL. Recrystallized mesh-rim texture with magnetite disseminations over the borders. Chromite is corroded and recrystallized in the grain margins. d.) Sample ELI-731-147.45 in PPL. e.) Sample ELI-512-34.80 in CPL. Thrust and folded banded serpentine vein. f.) Same association in PPL. Width of the photos = 1.6 mm.

4.5 Chromitites

Orthocumulate texture is observed in the samples with disseminated euhedral chromite (around 240 um) as the cumulate grains (Fig. 15a – d). Intercumulate grains are altered

up to 100%. The matrix is formed by different proportions of talc, serpentine, phlogopite, amphibole and carbonate. Distinction between phlogopite and talc is challenging due to similar optical properties, only easily differentiated when talc exhibits high third order interference colors (Fig. 15a – b), or when phlogopite is pleochroic and masked by magnetite (Fig. 15c – d), nonetheless presence of phlogopite is proved by microprobe analyses (Fig. 15a – b). Serpentine (interlocking textures and fibrous aggregates) and carbonate are more abundant in the matrix of ELI-436-112.00, where the amphibole content is lower. Coarser aggregates and amphibole grains are more abundant in ELI-453-42.10. Most crystals exhibit undulose extinction.

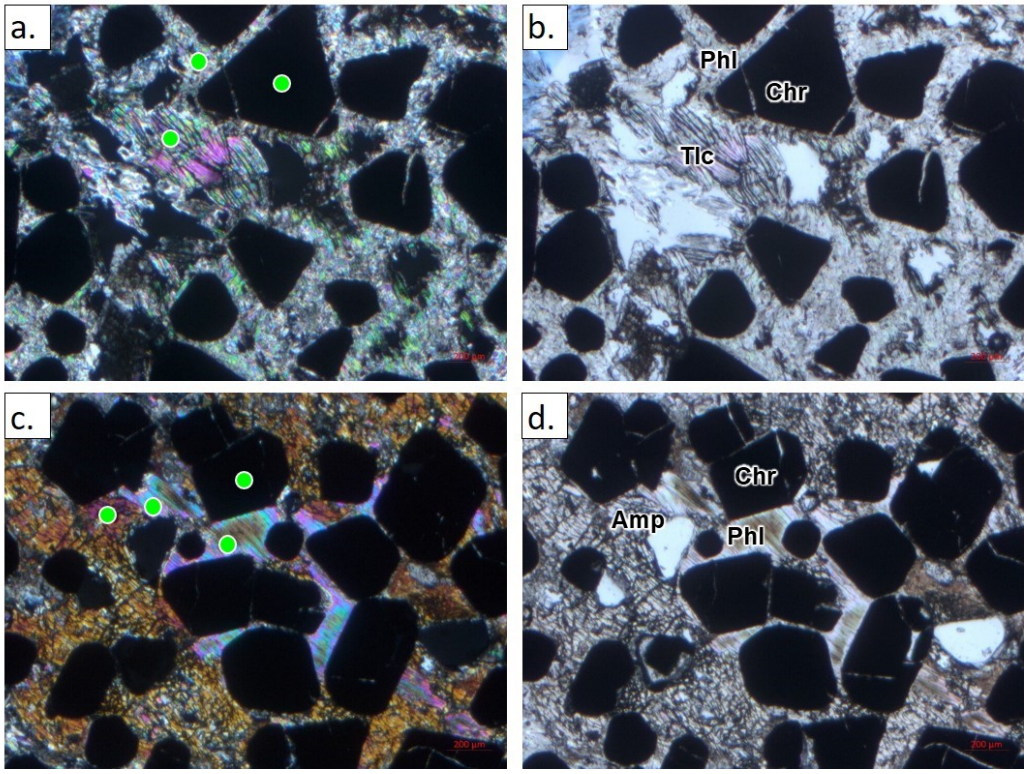

Figure 15. Sample ELI-453-42.10 of the chromitites. a.) Tabular talc aggregate (middle of the picture). Phlogopite is also recognized in the surrounding fine-grained matrix. b.) Same association in PPL. c.) Phlogopite (blue-purple colors) surrounded by amphibole altered pyroxene. d.) Same association in PPL. Phlogopite is slightly pleochroic. Electron microprobe measurements were taken in the areas highlighted with the green circles in pictures a.) and c.). Width of the photos = 2.2 mm.

5 MINERAL CHEMISTRY

Electron microprobe analyses were carried with a main focus on the alteration minerals and the chromite grains surrounded by them. Due to large amount of data, only two tables are presented in this section. Table 5 contains the major oxide compositions of relict minerals (without chromite) while Table 6 summarizes the major oxide compositions of the alteration minerals of the different lithologies, showing representative measurements. Complete tables can be found in Appendixes 10 to 18.

5.1 Relict minerals

5.1.1 Olivine

The analyzed olivine grains show quite homogenous composition, with only minor variations. Due to high degree of alteration, relict olivine mostly occur in the cumulate peridotites (least altered lithology), with few occurrences in other lithologies. Only 4 spots of olivine were analyzed, belonging to cumulate peridotites and chlorite peridotites. The Fo content of olivine in cumulate peridotites is ~ 82-83 mol% (similar to the observation of Alapieti et al., 1989; 3 analyzed points), whereas one olivine grain has Fo = 84.77 mol% in the chlorite peridotites (sample R25-23.5, point 9). The points measured in the cumulate peridotites belong to small relicts of olivine surrounded by green iron rich serpentine (Fig. 16a – b), while the relict of olivine in the chlorite peridotites has a halo of yellowish iron rich serpentine.

The minor difference is the slight higher MgO in olivine of chlorite peridotites (46.33 wt. % in chlorite peridotites and 44.84 wt. % average in cumulate peridotites), and a slight lower in FeO(total) and SiO_2 (FeO = 14.54 wt. % and SiO_2 = 39.71 wt. % in chlorite peridotites and FeO = 16.07 wt. % and SiO_2 = 40.6 wt. % average in cumulate peridotites; Table 5).

5.1.2 Clinopyroxene

Clinopyroxenes in the samples form part of the diopside-hedenbergite-augite series (Figs. 16c – d). Spots analyses were conducted in the chlorite, serpentine and pyroxene

peridotites. Composition of clinopyroxenes are fairly consistent (Table 5). Point R22.2-72 1 has the highest content of CaO and its composition is close to the composition of the Diopside end member. Point R22-3-87 2 has notorious higher content of FeO. Nevertheless, the latter is being partially replaced by magnetite.

It is also observed that some of the clinopyroxene grains have rather high Cr_2O_3 of up to 1.14%.

5.1.3 Apatite

Apatite is observed as an accessory mineral, only in sample ELI-670-15.50 (point 1, Table 5) as an elongated prismatic crystal. Apatite is mainly surrounded by amphibole and in less proportion by serpentine, phlogopite and carbonate (Fig 16e – f).

Table 5. Electron microprobe results of relicts. Fo is given for olivine and Mg# for clinopyroxene

Lithology	Na_2O	CaO	Cr_2O_3	P_2O_5	MgO	FeO	MnO	K_2O	Al_2O_3	NiO	TiO_2	SiO_2	Total	Fo/Mg#	Sample - Point	Mineral
Cumulate peridotites	0.01	0.06	0.00	0.00	44.68	15.77	0.19	0.01	0.01	0.17	0.01	40.40	101.31	83.24	ELI-67-9.30-9.40 5	Olivine
	0.07	0.04	0.02	0.04	44.89	16.61	0.26	0.02	0.00	0.19	0.02	40.46	102.60	82.55	ELI-67-9.30-9.40 6	Olivine
	0.05	0.10	0.00	0.03	44.95	15.83	0.27	0.03	0.02	0.18	0.00	40.93	102.38	82.22	ELI-83-477-47.8 9	Olivine
Chlorite peridotites	0.17	22.43	0.37	0.03	17.63	3.73	0.06	0.04	0.18	0.02	0.06	53.74	98.43	0.89	ELI-671-13.50 1	Clinopyroxene
	0.66	22.97	1.14	0.04	15.74	3.96	0.12	0.04	3.41	0.02	0.29	52.58	100.98	0.88	ELI-671-13.50 2	Clinopyroxene
	0.03	0.09	0.21	0.03	46.33	14.54	0.18	0.00	0.00	0.10	0.05	39.71	101.27	84.77	R25-23.5-9	Olivine
Serpentine peridotites	0.03	26.43	0.07	0.00	17.77	2.20	0.05	0.00	0.00	0.02	0.00	56.29	102.87	0.93	R22.2-72 1	Clinopyroxene
	0.54	23.31	0.93	0.00	16.12	4.53	0.13	0.01	2.91	0.01	0.33	53.24	102.06	0.86	R22.2-72 4	Clinopyroxene
	0	54.35	0	41.56	0.4	0.249	0.009	0.006	0	0.017	0.011	0.027	96.63		ELI-670-15.50 1	Apatite
Pyroxene peridotites	0.36	18.44	1.08	0.00	14.58	16.91	0.15	0.01	1.91	0.03	0.24	44.28	97.99	0.61	R22-3-87 2	Clinopyroxene
	0.50	20.46	1.11	0.04	16.66	4.44	0.10	0.01	3.69	0.00	0.23	50.83	98.06	0.87	R22-3-87 3	Clinopyroxene
	0.51	22.90	0.86	0.03	16.05	4.18	0.08	0.00	2.91	0.01	0.83	52.57	100.92	0.87	R22-3-87 8	Clinopyroxene
	0.77	22.48	1.07	0.01	15.05	4.33	0.07	0.01	3.65	0.03	0.32	51.66	99.44	0.86	R22-3-87 10	Clinopyroxene

Table 6. Representative major elements composition of alteration minerals determined by electron microprobe.

Lithology	Na_2O	CaO	Cr_2O_3	P_2O_5	MgO	FeO	MnO	K_2O	Al_2O_3	NiO	TiO_2	SiO_2	Total	Sample - Point	Mineral
Serpentine peridotites	0.01	0.00	1.14	0.00	29.13	8.80	0.09	0.25	13.29	0.12	0.15	33.17	86.15	ELI-675-27.50 7	Chlorite
Pyroxene peridotites	0.04	0.08	0.30	0.00	27.81	9.63	0.04	0.21	12.49	0.09	0.00	32.71	83.40	ELI-675-54.10 5	Chlorite
Amphibole pyroxenites	0.05	0.07	0.12	0.00	26.31	11.90	0.10	0.12	16.17	0.09	0.04	31.14	86.10	ELI-670-52.50 1	Chlorite
Cumulate peridotites	0.86	13.59	1.14	0.03	21.26	3.27	0.04	0.02	3.01	0.05	0.15	55.25	98.67	ELI-67-9.30-9.40 10	Amphibole
Chromitites	0.26	13.28	0.72	0.00	23.30	1.11	0.04	0.04	1.44	0.08	0.01	57.03	97.31	ELI-453-42.10-5	Amphibole
Amphibole pyroxenites	0.48	12.10	0.00	0.00	21.77	4.80	0.24	0.01	0.51	0.02	0.01	57.93	97.87	ELI-672-34.00 6	Amphibole
Cumulate peridotites	0.04	0.34	0.00	0.00	25.90	15.75	0.31	0.03	0.20	0.00	0.03	37.97	80.57	ELI-83-477-47.8 4	Serpentine
Serpentine peridotites	0.01	0.02	0.00	0.00	32.93	8.93	0.12	0.01	1.55	0.07	0.00	42.19	85.82	ELI-675-27.50 8	Serpentine
Serpentinites	0.04	0.00	0.04	0.00	39.84	1.23	0.04	0.02	1.16	0.10	0.04	44.35	86.86	ELI-731-147.45-50 5	Serpentine
Chlorite peridotites	0.00	52.60	0.00	0.00	2.65	0.64	0.34	0.00	0.33	0.01	0.01	1.03	57.61	ELI-671-13.50 5	Calcite
Pyroxene peridotites	0.00	58.07	0.00	0.03	1.25	0.55	0.63	0.04	0.00	0.02	0.00	0.00	60.59	ELI-47-20.57-70 4	Calcite
Chlorite peridotites	0.06	28.76	0.01	0.02	18.09	3.66	0.74	0.01	0.47	0.00	0.00	0.89	52.69	ELI-674-26.25 8	Dolomite
Serpentine peridotites	0.00	30.09	0.00	0.02	18.62	2.30	0.58	0.02	0.01	0.00	0.03	0.00	51.66	ELI-670-15.50 5	Dolomite
Cumulate peridotites	1.01	0.00	1.52	0.00	23.37	6.18	0.06	7.07	15.11	0.07	3.28	37.80	95.47	ELI-67-9.30-9.40 8	Phlogopite
Chromitites	0.20	0.00	2.54	0.00	23.72	1.26	0.00	10.30	15.01	0.25	0.89	40.29	94.46	ELI-453-42.10-4	Phlogopite
Amphibole pyroxenites	0.06	0.05	0.80	0.00	23.73	11.69	0.15	4.44	13.81	0.10	1.09	33.94	89.85	ELI-672-45.60-6	Phlogopite
Chromitites	0.06	0.03	0.04	0.00	30.87	0.60	0.00	0.01	0.04	0.12	0.01	62.24	94.02	ELI-453-42.10-8	Talc
Talc pyroxenite	0.32	0.00	0.33	0.00	28.28	4.35	0.02	0.07	1.51	0.05	0.03	58.74	93.72	R25-3-27 3	Talc

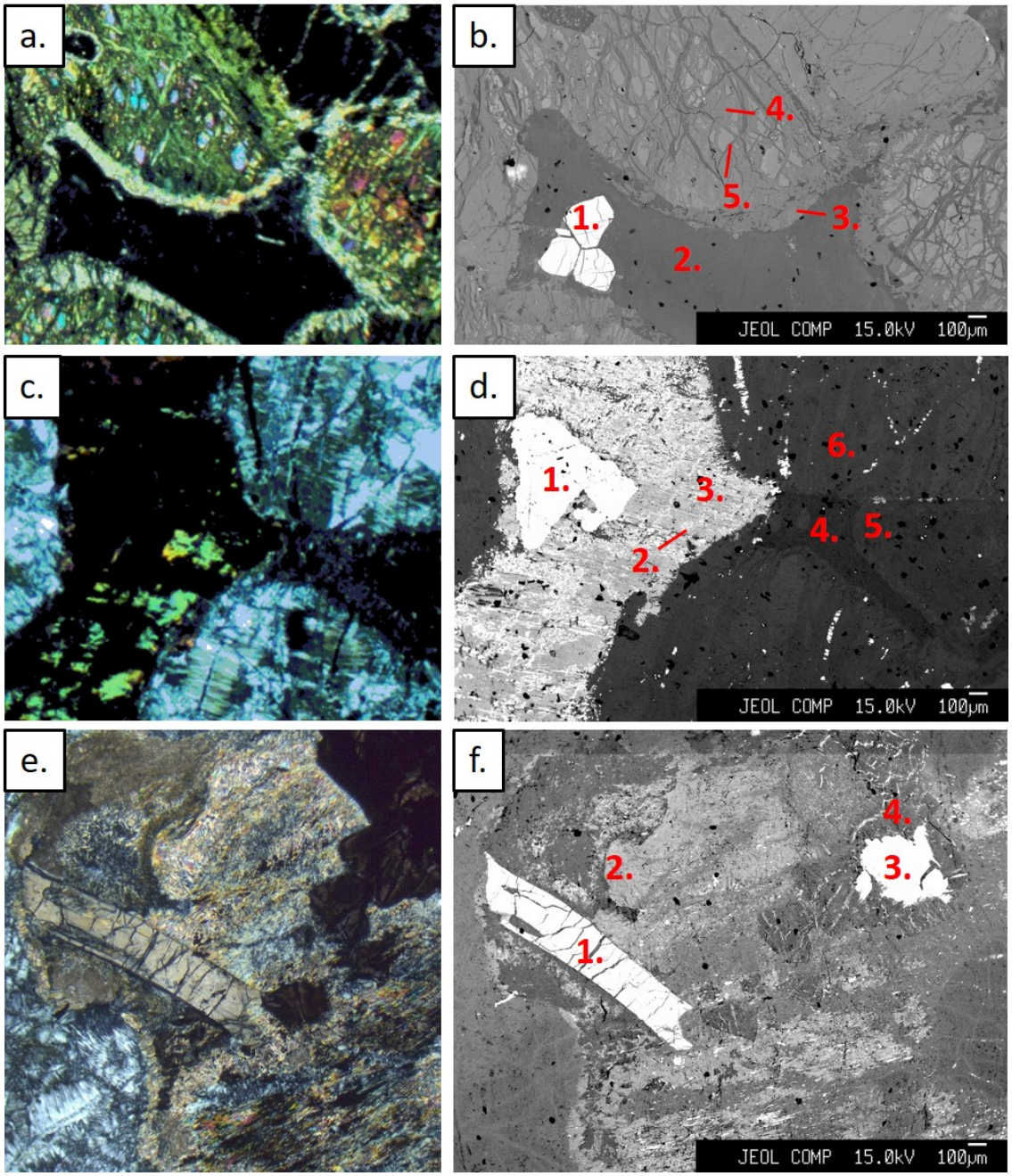

Figure 16. a.) XPL photo of sample ELI-67-9.30-9.40 of the cumulate peridotites. b.) Back-scatter image of the same area as a. 1 = chromite, 2 = chlorite, 3 = amphibole, 4 = serpentine, 5 = olivine. c.) XPL photo of sample R22-3-87 of the pyroxene peridotites. d.) Back-scatter image of the same area as c. 1 = chromite, 2 = clinopyroxene, 3 = clinopyroxene, 4 = chlorite, 5 = chlorite and 6 = serpentine. e.) XPL photo of sample ELI-670-15.50 of the serpentine peridotites. f.) Back-scatter image of the same area as e. 1 = apatite, 2 = amphibole, 3 = chromite, 4 = chlorite.

5.1.4 Chromite

Chromite is present in the peridotites as a cumulus mineral. Chromite is the best preserved primary crystal in altered lithologies with only partial alteration along cracks and rims of

the grains, and occasional recrystallization at the borders. The alteration of chromite grains seems to be less intense in chromitites than in peridotites (Fig. 17). Exact probing of the alteration rim is difficult, as the rim has a size of less than 10 μm (e.g. in chromitites).

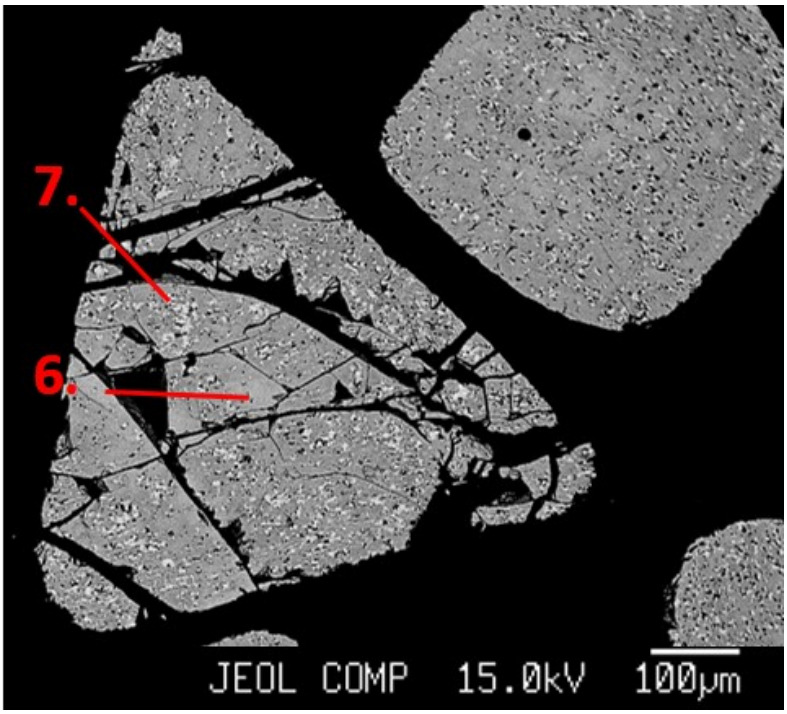

Figure 17. Back-scatter image of chromitite (sample ELI-453-42.10). 6 = chromite, 7 = alteration product of chromite. Optical microscope picture of the same association can be seen in Figure 9, a & b of the petrography chapter.

As stated in Alapieti et al., (1989), Cr_2O_3, Al_2O_3 and MgO are observed to decrease towards the rims of the grains, contrary to FeO. Nonetheless, an exception was observed in the chromitite sample where Cr_2O_3 increases towards the small chromite rims with a decrease in Al_2O_3, MgO and FeO.

The compositional difference between fresh cores and altered rims is variable. For example, some chromite grains have small differences in Cr_2O_3 between rim and core (e.g. 1.37 wt%; sample ELI-675-54.10 points 1 and 2; Fig. 18a), and some grains have large compositional differences (e.g. 26.11 wt%; sample ELI-673-20.10, points 8 and 8.5; Fig. 18b). Alteration rims also have large compositional variations. In sample R25-23.5 (points 1 and 2; Fig. 18c), Cr_2O_3 varies from 35.71 to 18.59 wt% in the alteration rim, and in another grain from the same sample (points 6 and 7; Fig. 18d), it varies from 35.17 to 0.57 wt%. Alteration rims are mostly composed of FeO.

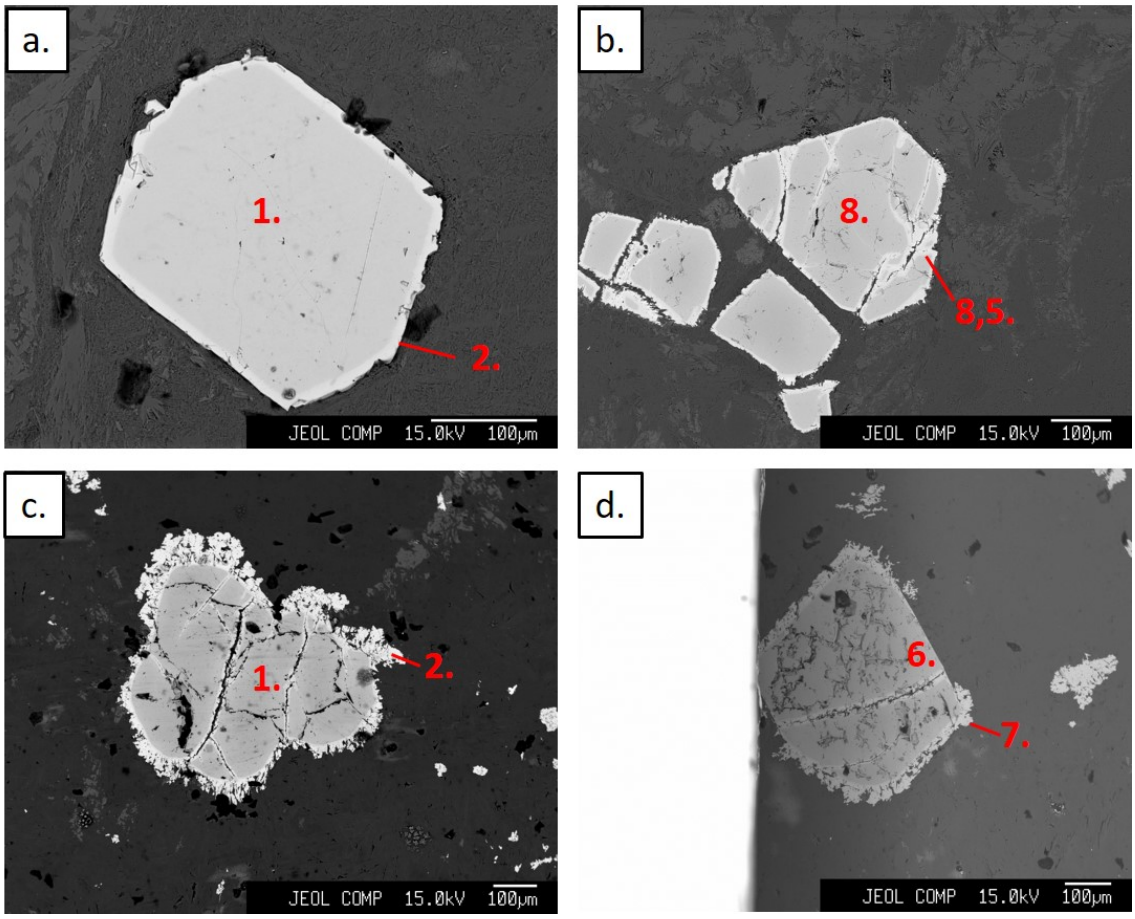

Figure 18. Back-scatter image of different chromite grains. a.) Sample ELI-675-54.10; 1 = chromite, 2 = chromite rim. b.) Sample ELI-673-20.10; 8 = chromite, 8,5 = chromite rim. c.) Sample R25-23.5; 1= chromite, 2 = chromite rim. d.) Sample R25-23.5; 6 = chromite, 7 = chromite rim.

5.1.5 Phlogopite

Phlogopite is recognized as an intercumulus mineral of tabular aggregates, often observed in the vicinities of chromite grains and occasionally being replaced by chlorite (Figs. 16, e and f, point 4). Phlogopite is recognized in both peridotites and pyroxenites as well as in chromitites. The compositions of phlogopite vary slightly. Phlogopite has the generally high K_2O, Cr_2O_3 and TiO_2 contents. Amongst phlogopite of the studied different lithologies, phlogopites in chromitites have the highest Cr_2O_3, Al_2O_3, MgO, NiO and the lowest FeO and TiO_2. FeO in phlogopite is considerably higher in pyroxene peridotites and pyroxenites, it is also worth to mention that phlogopite generally contain disseminated very fine grained magnetite.

5.2 Alteration minerals

5.2.1 Chlorite

Chlorite (clinochlore) is present in most of the lithologies, occurring mainly as an alteration product of intercumulus minerals (Fig. 16). This alteration mineral show large compositional variations. Generally, the MgO content in chlorites show negative correlation with FeO and Al_2O_3 throughout all the samples. Chlorites have higher CaO and Na_2O contents in cumulate peridotites compared to other lithologies (<0.77 wt. % vs. <0.49 wt. %). Even in the cumulate peridotite, chlorite show some compositional variation in K_2O, Na_2O and Al_2O_3 (e.g., <0.07 wt. % , <0.027 wt. % and <15.53 wt. % In ELI-67-9.30-9.40, while <0.74 wt. % , <0.49 wt. % and <19.19 wt. % in ELI-83-477-47.8). On the opposite, MgO contents are higher in ELI-67-9.30-9.40 (<30.18 wt. %) compared to ELI-83-477-47.8 (<26.76 wt. %).

It can also be observed that chlorite in the metaperidotites have higher MgO contents, and lower FeO than that in the pyroxenites. Some of the observed chlorite aggregates have high content of Cr_2O_3 (<1.42 wt. %). They occur sporadically in the lithologies and they are observed either surrounding chromite grains or replacing pyroxene grains which are in contact with chromite grains.

5.2.2 Amphibole

Amphibole occurs as a replacement mineral of pyroxene and serpentine (either masking the crystals or as fine-grained aggregates), and as rims of former pyroxene and olivine crystals (Figs 16, a-b and e-f). Amphibole is also recognized sporadically in veins. Amphibole in the samples belong almost entirely to the tremolite - actinolite series, with the exception of a K-bearing pargasite found in the amphibole pyroxenite, occurring as a tabular aggregate with actinolite.

Cr_2O_3 and Al_2O_3 are slightly positively correlated. Other amphiboles with elevated Cr_2O_3 content are recognized in altered intercumulus pyroxene which contains chromite crystals. It is also observed that Cr_2O_3 contents in amphibole are generally higher in the alteration product of intercumulus pyroxene, than in the alteration product of serpentines.

Furthermore, the FeO and MnO contents of amphiboles are higher in pyroxenites than in peridotites, whereas MgO is lower.

5.2.3 Serpentine

Serpentine is the most common mineral in the peridotites and occurs as an accessory mineral in the pyroxenites. Serpentine is observed in mesh, bastite, interlocking/interpenetrating textures and in veins (Figs 16, a-b and c-d). The composition of serpentine is relatively homogenous in all of the samples, and there is minor variations in major element compositions regardless of textures of serpentine (e.g. serpentine flakes have variable MgO content ranging from 38 wt. % to 33 wt. %). Nonetheless, serpentine aggregates with elevated FeO show different anomalous colors. For example, serpentines with FeO <17.28 wt. % in cumulate peridotites show green colors in PPL and anomalous colors in CPL which gave serpentine a very similar appearance to chlorite. Meanwhile, serpentines in chlorite and serpentine peridotites with FeO <22.27 wt. % show yellowish colors in both PPL and CPL.

It is also observed that serpentines of sample ELI-731-147.45-50 (serpentinites) have the highest values of MgO (<39.79 wt. %), as its protolith, may be an adcumulate dunite with high percentage of olivine.

5.2.4 Carbonates

Carbonates were probed in chlorite, amphibole, serpentine and pyroxene peridotites. This mineral is observed as veins and very-fined aggregates, composed of both calcite and dolomite. Distinction from one another is not possible through petrography due to similar textures and optical features. Carbonates show an inverse relation between CaO and MgO. Some carbonates show high contents of SiO_2, most likely due to the presence of very fine grained silicate phases (such as chlorite and serpentine; e.g. ELI-673-20.10 point 9 of the pyroxene peridotites).

5.2.5 Talc

Talc is mostly recognized as very fine grained aggregates. Talc is also observed as tabular

aggregates in chromitites (Fig. 9, petrography chapter). Talc in chromitites and pyroxenites have generally similar composition, but the MgO and NiO contents are higher in chromitites than in pyroxenite, and the Cr_2O_3, FeO, and Al_2O_3 contents are lower in the former.

6 DISCUSSION

6.1 Hydrothermal alteration

All of the studied samples show strong signs of hydrothermal alteration activity. Even though alteration is observed with different intensities and the alteration minerals occurring in different amounts, the same mineral assemblages occur throughout almost all different lithologies. The identified hydrothermal alteration minerals include serpentine, chlorite, amphibole, magnetite, talc and carbonate.

The dominant alteration minerals are serpentine for the peridotites and, amphibole and talc for the pyroxenites. Both lithologies share similar percentages of chlorite. Considerably stronger serpentine alteration is observed in some of the peridotites, hence, those rocks are grouped as “serpentinites”. The silicate phases in the chromitites are altered in a similar manner to the pyroxenites.

Different stages of alteration can be broadly defined via textural relations, which are mentioned in the following lines. Pseudomorphic serpentine textures indicate the first stage of alteration (Wicks and Whittaker, 1977). The observed pseudomorphic textures were mesh-rim (olivines) and bastite replacements (pyroxenes). “Fresh” mesh-rim textures were almost restricted to the cumulate peridotites which are the least altered samples of this study. Based on the conclusion of Wicks and Whittaker (1997) and the identification methods in Wicks and O’Hanley (1988), mesh cores in cumulate peridotites are most likely lizardite, whereas the fibrous and flake aggregates in almost the remaining samples are either chrysotile or antigorite.

Olivine grains are frequently rimmed by serpentine flakes. These serpentine flakes are partly masked by amphibole. In some of the samples, bastite in a slightly altered pyroxene is also partly mantled by chlorite.

In every other lithologies besides the cumulate peridotites, non-pseudomorphic texture of serpentine is the dominant type, indicating recrystallization of serpentine. In some of the samples, the core of olivine grains are observed being replaced by amphibole and less commonly by chlorite. Amphibole alteration is also recognized in recrystallized bastites, intergrown with flakes and in aggregates with a sort of chessboard texture. Commonly, amphibole rims are recognized growing outwards from the altered grains.

Olivine and pyroxene grains are also altered to magnesium carbonate and talc. Carbonate usually forms a second layer surrounding amphibole rims and/or as disseminations throughout the sample. Carbonate occurs in filling fractures more than in crosscutting veins. Talc seems to be intrinsically related to carbonate. Frequently, when talc is observed, at least, minor quantities of carbonate are recognized. The close correlation between talc and carbonate can also be recognized in Elijärvi's main chromitite layer (Alapieti, 1989).

An alteration sequence is thus defined for the host rocks of the Kemi deposit, based on the aforementioned characteristics (Fig. 19). Overlapping of alterations as well as more advanced stage alteration could have taken place depending on the intensity of alteration. Nonetheless, we suggest a sequence which may represent the most likely hydrothermal fluid activities occurred in Kemi.

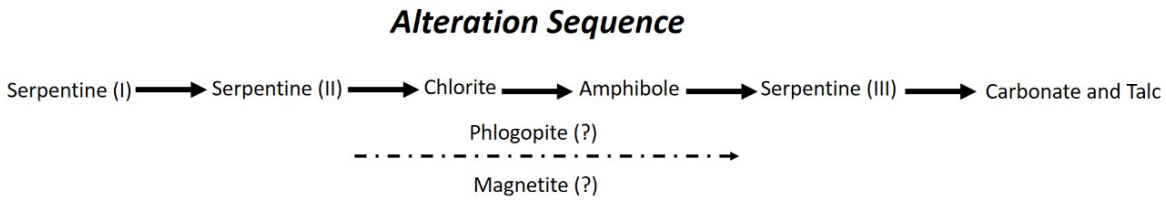

Figure 19. Proposed alteration sequence.

A main stage of serpentinization is proposed as the first alteration event, where pseudomorphic textures of serpentine was developed. This was followed by a second stage of serpentinization that produced non-pseudomorphic textures of serpentine (flake and fibrous aggregates). Consequently, serpentine was overprinted by chlorite alteration, evidenced by the mantling of pseudomorphic textures, vaguely in non-pseudomorphic textures and by the occurrences of chlorite aggregates in the "chlorite intercumulus",

resembling serpentine interpenetrating and interlocking textures. Chlorite alteration is followed by amphibole alteration. Amphibole is recognized overprinting serpentine flakes in olivine and pyroxene rims, olivine cores and recrystallized bastite. On the other hand, chlorite alteration over amphibole was not recognized in any of the samples, therefore a later timing for amphibole alteration is proposed.

A third episode of serpentinization could also be possible. Evidence for this might be the occurrence of bastite rims on flaky serpentine –product of amphibole serpentinization. Occurrence of "chessboard" intergrowths of bastite and amphibole could either be related to this episode of serpentinization (amphibole to serpentine) or to the second stage amphibole alteration. The third episode of serpentinization might also be related to later crosscutting veins of serpentine (veins of serpentine with interpenetrating textures and veins of serpentine with banded textures). Later serpentine veins are observed being cut and altered to carbonate exclusively. As mentioned above, talc and carbonate alteration is assumed to occur coevally. Hence, carbonate and talc alteration presumably postdate both amphibole alteration and the later episode of serpentinization.

No timing relation for magnetite was observed. Magnetite is a common product of serpentine alteration (Wicks and Whittaker, 1977; Paulick et al., 2006), thus it might have occurred alongside with serpentinization in every stage. Phlogopite is considered to be a primary mineral based on textural relations, nonetheless more studies would be needed to assess this statement with full certainty. If phlogopite occurred as a secondary mineral, its alteration would be uncertain since it does not appear to share any relation with any other alteration mineral. It was only identified that phlogopite occurs as an intercumulus mineral and that it is frequently surrounding chromite grains.

The lower contents of other alteration minerals besides serpentine in serpentinites might be related to hydrothermal fluids containing less amounts of silica (Paulick et al., 2006).

6.2 Spatial distribution

Different variations in features (primary and secondary) can be recognized from the analyzed samples. The array of samples used in this study constrain a wide area of the Kemi intrusion. The samples belong to boreholes located in 12 different cross sections

which span a distance from the first one (6500) to the last one (7350) of 850 m (Fig. 20). The samples come from 17 boreholes (Figs. 21 and 22). Changes in textures, mineral composition and mineral chemistry were revised in function of the distance from the samples to the main chromitite ore zone in order to determine the spatial relationship.

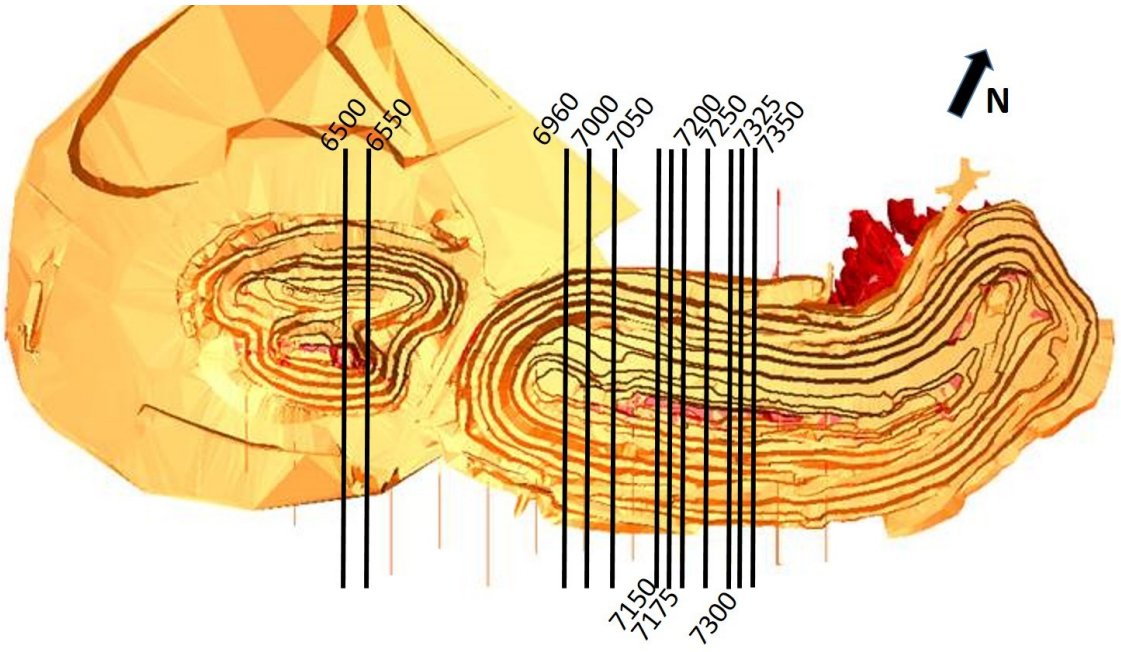

Figure 20. Plain view of Kemi mine open pit displaying the cross sections from which this study samples originate.

It is observed that chlorite in samples of the cumulate peridotites show a decrease of Al_2O_3, K_2O and Na_2O with more proximity to the chromitite ore zone. Nevertheless this relation was not observed in any other peridotite nor pyroxenite. In cross section 7000 (borehole R22), serpentine, carbonate and talc seem to increase with proximity to the ore, while in cross section 7250 (borehole ELI-675) similar trend is observed. This variations were only observed in the mentioned cross sections and are not recognized in the other cross sections or boreholes where the behavior of the alterations were more erratic, or in the case of amphibole alteration, the increase would be related to proximity to layers of amphibole pyroxenites. Although no apparent trend in serpentine alteration in peridotites was observed, all of the four serpentinite samples were located in the areas close to the ore zone.

It is also observed from the microprobe analyses that many of the different alteration minerals contain high concentrations of Cr_2O_3 (e.g. 1.1% in chlorite of sample ELI-675-

27.50, 0.6% in amphibole of sample ELI-673-71.4), nevertheless this concentrations show no relation with depth nor proximity to the ore, thus it is more feasible that this concentrations reflect high % Cr_2O_3 of the primary minerals (e.g. pyroxene). Nonetheless, it is observed in one amphibole vein of sample ELI-67-9.30-9.40 (Fig. 21; <40 m away from a chromitite layer) of the cumulate peridotites, contain rather high concentrations of Cr_2O_3 (1.4%).

The only relatively constant pattern observed in the samples was the increase in the color order of amphibole in CPL with proximity to the ore, but it should still be taken into account that this variation could be related to talc alteration and most of the samples are considerably far from the chromitite layers.

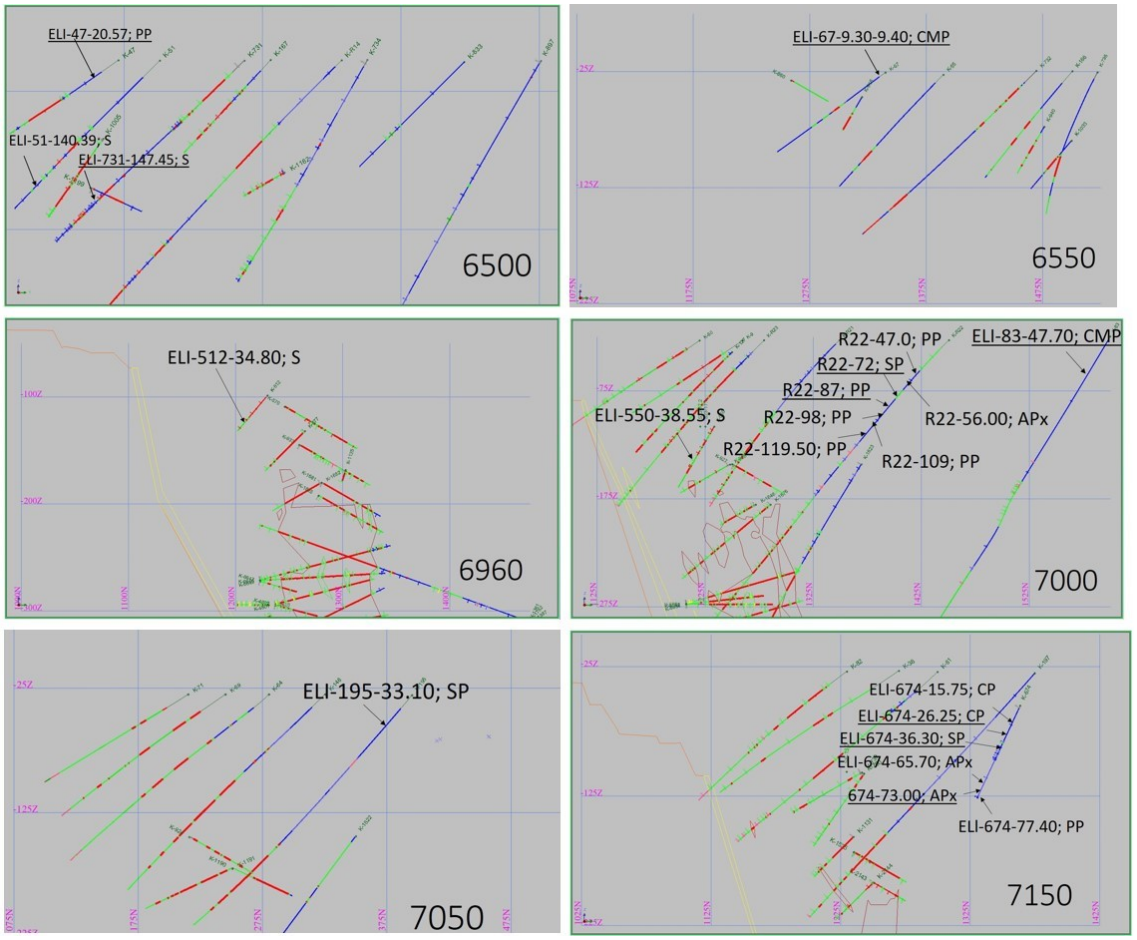

Figure 21. Cross sections 6500, 6550, 6960, 7000, 7050 and 7150 (indicated by the lower – right corner number) with the location of each sample. Each grid square is of 100m x 100m. Colors from the drill hole logs are given as following; red = chromite ore and serpentine based ore, green = talc – carbonate rock and blue = altered ultramafic rocks. APx = amphibole pyroxenite, CMP = cumulate peridotites, CP = chlorite peridotites, PP = pyroxene peridotites, SP = serpentine peridotites and S = serpentinites.

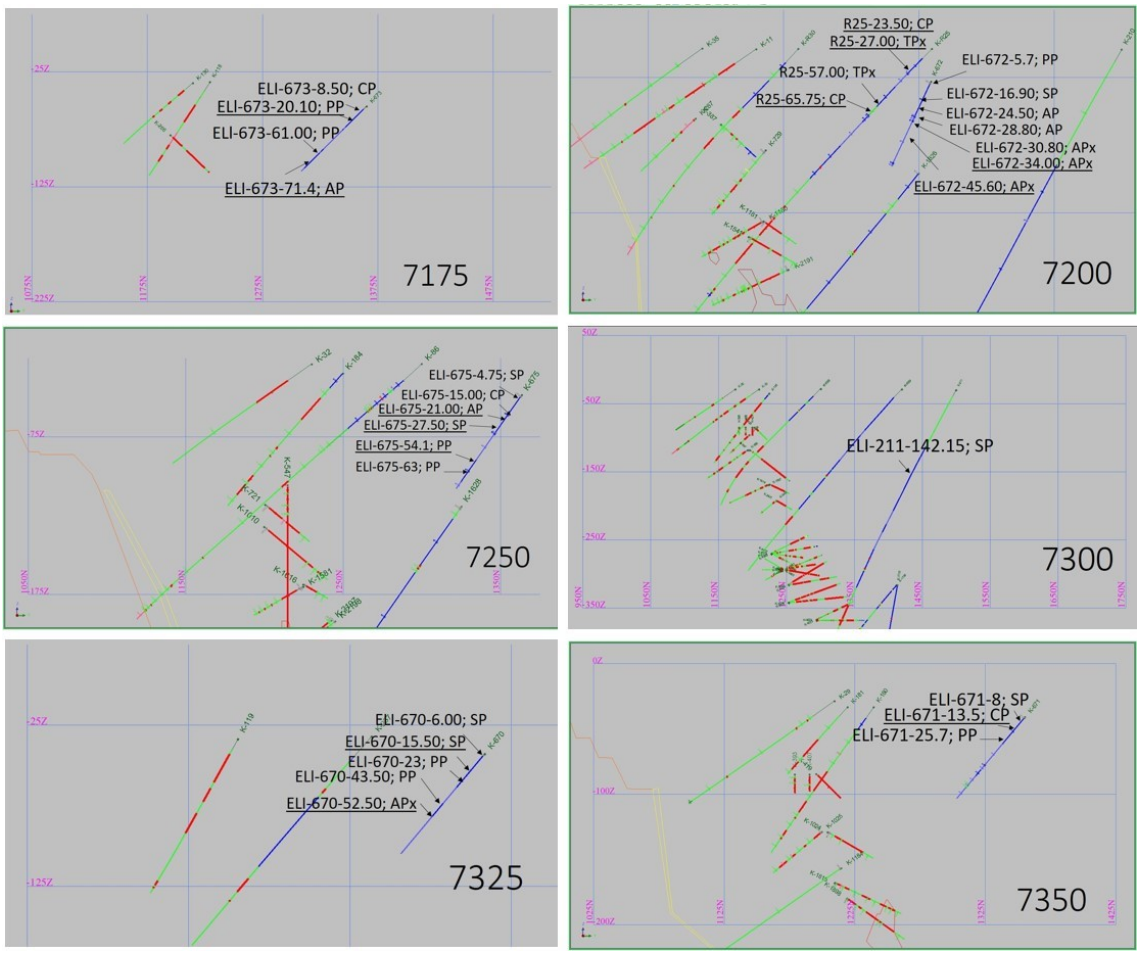

Figure 22. Cross sections 7175, 7200, 7250, 7300, 7325 and 7350 (indicated by the lower – right corner number) with the location of each sample. Each grid square is of 100m x 100m. Colors from the drill hole logs are given as following; red = chromite ore and serpentine based ore, green = talc – carbonate rock and blue = altered ultramafic rocks. AP = amphibole peridotites, APx = amphibole pyroxenite, CP = chlorite peridotites, PP = pyroxene peridotites, SP = serpentine peridotites and TPx = talc pyroxenites.

6.3 Fluid source

Rocks in the Kemi intrusion are altered the most in the lower and upper parts. The basal series are formed by mylonitic talc-chlorite-carbonate schist. Ultramafic rocks above the basal series are variably altered to serpentine, talc-carbonate and less proportions amphibole and chlorite. Different episodes of alteration are evidenced in petrographical features in the aforementioned order. Initial alteration produced by hydration of the rocks is serpentine with pseudomorphic textures. Although exact timing of the alteration cannot be properly constrained with this work's material, it can be concluded that the fluid evolved towards higher contents of SiO_2 (SiO_2 = ~37.6 wt. % in pseudomorphic serpentine and SiO_2 = ~41.7 wt. % in non pseudomorphic serpentine) and higher PT conditions, evidenced in the occurrences of antigorite and other alteration assemblages.

Talc and carbonate alterations could represent alterations related to retrograde metamorphism. The direct source of fluid is difficult to constrain from this study. The presence of mylonites and schist in the basal portions suggests the occurrences of deformation that could have provided the pathways for fluids in the lower portions of the intrusion, resulting in pervasive alterations, probably in the Svecofennian orogenic process.

7 CONCLUSIONS

Kemi layered intrusion is altered in the lower and upper parts of the intrusion. In the samples of the intensely altered ultramafic portion (lower part) six alteration events were identified: serpentine alteration (development of pseudomorphic textures), a second episode of serpentine alteration (development of non-pseudomorphic textures), chlorite alteration, amphibole alteration, a third episode of serpentine alteration and at last, an episode of talc-carbonate alteration. Alterations could have been intensified during Svecofennian Orogenic event. Mineralogy of the alterations as well as the mineral chemistry suggests the evolution of the fluid towards more silica rich compositions.

Compositions of the major elements in alteration minerals proved to be relatively uniform with slight variations (e.g. high Cr_2O_3 bearing silicates). Variations in primary and secondary minerals (e.g. chromite content of the sample and abundance of a certain alteration minerals) in the samples were also recognized. Nevertheless this variation did not seem to respond to proximity to the ore, but could be more related to protolith compositions. Nonetheless, the existence of a spatial distribution of variations in alteration minerals and mineral chemistry with proximity to the ore cannot be ruled out since the majority of the samples used in this study were relatively far from the ore.

In order to obtain a better understanding of the occurrence of alteration, its possible spatial distribution, fluid source and pathways, petrographical, geochemical and isotopic studies are required for samples spanning a wider area (including areas surrounding the chromitite layers).

8 AKNOWLEDGEMENTS

This project was funded by K. H. Renlund foundation, Finland. Holger Paulick, Sari Grönholm and Timo Huhtelin are acknowledged for providing material and information which were crucial for the development of this work. I want to give my gratitude to Sheng-Hong Yang for his supervision on this project and to Leena Palmu from the Center of Microscopy and Nanotechnology for her collaboration with the microprobe analyses. This project was also greatly benefited from the unconditional support and critics from friends and colleagues at the University of Oulu.

To my family, all of my success is thanks to your efforts.

To Ilayda, thanks for your endless support.

9 REFERENCES

Alapieti, T.T., Kujanpaa, J., Lahtinen, J.J., & Papunen, H. (1989). The Kemi stratiform chromitite deposit, northern Finland. Economic Geology 84, 1057-1077.

Alapieti, T.T., Huhtelin, T. A. (2005). The Kemi intrusion and associated chromitite deposit. Field trip guidebook: Early Paleoproterozoic (2.5-2.4) Tornio-Näränkävaara layered intrusion belt and related chrome and platinum group element mineralization, Northern Finland. Ed. by Alapieti & Kärki. Geological survey of Finland. Guide nr. 51a. Espoo, p. 13-31.

Alt, J. C., Shanks, W. C., Bach, W., Paulick, H., Garrido, C. J.; Beaudoin, G. (2007). Hydrothermal alteration and microbial sulfate reduction in peridotite and gabbro exposed by detachment faulting at the Mid-Atlantic Ridge, 15°20′N (ODP Leg 209): A sulfur and oxygen isotope study. Geochem. Geophys. Geosyst. 8(8), Q08002, doi:10.1029/2007GC001617.

Bach, W., Garrido, C. J., Paulick, H., Harvey, J., and Rosner, M. (2004). Seawater-peridotite interactions: First insights from ODP Leg 209, MAR 15_N, Geochem. Geophys. Geosyst., 5, Q09F26, doi:10.1029/2004GC000744.

Cawthorn, R. G., Barnes, S. J., Ballhaus, C. & Malitch, K. N. (2005). Platinum-group element, chromium, and vanadium deposits in mafic and ultramafic rocks. Economic Geology, 100th Anniversary Volume 215–249.

Cawthorn, R. G. (2015). The Bushveld Complex, South Africa. In: Charlier, B., Namur, O., Latypov, R. & Tegner, C. (eds) Layered Intrusions, 1st edn. Springer, pp. 517–588.

Eales, H. V. (2000) Implications of the chromium budget of the western limb of the Bushveld Complex. S. Afr. J. Geol. 103:141–150.

Eales, H. V. (2002) Caveats in defining the magmas parental to the mafic rocks of the Bushveld Complex, and the manner of their emplacement: review and commentary. Miner. Mag. 66 : 815–832.

Grönholm, S., (1994). Influence of mineral composition and microstructures on the mechanical properties of host rocks of the Kemi (Elijärvi) chromite deposit, Finland. Geological Survey of Finland – GTK, Report 126, 36pp.

Hanski, E., Huhma, H. (2005). Central Lapland greenstone belt. In: Lehtinen, M., Nurmi, P. A., Rämö O.T. (Eds.), The Precambrian Geology of Finland – Key to the Evolution of the Fennoscandian Shield. Elsevier B.V., Amsterdam, pp. 139-194.

Hibbard, M. J. (1995). Petrography to petrogenesis. Prentice Hall, edits. 587 pp.

Huhtelin, T. (2015) The Kemi chromite deposit. In: Maier WD, O'Brien H, Lahtinen R (eds) Mineral deposits of Finland. Elsevier, Amsterdam, pp. 133–162.

Iljina, M., Hanski, E. (2005). Layered mafic intrusions of the Tornio-Näränkävaara belt. In: Lehtinen, M., Nurmi, P. A., Rämö O.T. (Eds.), The Precambrian Geology of Finland – Key to the Evolution of the Fennoscandian Shield. Elsevier B.V., Amsterdam, pp. 101-138.

Irvine, T. N. (1975) Crystallization sequences in the Muskox intrusion and other layered intrusions: II origin of chromitite layers and similar deposits of other magmatic ores. Geochim. Cosmo. Acta 39 : 991–1020.

Irvine, T. N. (1977) Origin of chromitite layers in the Muskox intrusion and other stratiform intrusions: a new interpretation. Geology 5 : 273–277.

Laajoki, K. (2005). Karelian supracrustal rocks. In: Lehtinen, M., Nurmi, P.A., Rämö, O.T. (Eds.), The Precambrian Geology of Finland – Key to the Evolution of the Fennoscandian Shield. Elsevier B.V., Amsterdam, pp. 279–342.

Lauri, L., S., Andersen, T., Hölttä, P., Huhma, H., Graham, S. (2011). Evolution of the Archaean Karelian Province in the Fennoscandian Shield in the light of U–Pb zircon ages and Sm–Nd and Lu–Hf isotope systematics. Journal of the Geological Society, DOI 10.1144/0016-76492009-159

Le Maitre, R. W. (2002). Igneous Rocks: a Classification and Glossary of Terms: Recommendations of the International Union of Geological Sciences Subcommission on the Systematics of Igneous Rocks. Cambridge: Cambridge University Press, 236 pp.

Lenaz, D., Garuti, G., Zaccarini, F., Cooper, R., W. and Princivalle, F. (2012). The Stillwater Complex chromitites: the response of chromite crystal chemistry to magma injection. Geologica Acta, 10:33-41.

Li, C., Ripley, E. M., Oberthür, T., Miller, J. D. Jr., and Joslin, G. D. (2008). Textural,

mineralogical and stable isotope studies of hydrothermal alteration in the Main Sulfide Zone of the Great Dyke, Zimbabwe and the Precious Metals Zone of the Sonju Lake Intrusion, Minnesota, USA. Mineralium Deposita, vol. 43. pp. 97-110.

Maier, W. D., Barnes, S. J. (2008) Platinum-group elements in the UG1 and UG2 chromitites, and the bastard reef, at impala platinum mine, western Bushveld Complex, South Africa: evidence of late magmatic cumulate instability and reef constitution. Geol. Soc. S. Afr. 111 : 159–176.

Maier, W. D., Barnes, S. J., Groves, D. I. (2012) The Bushveld Complex, South Africa: formation of platinum, palladium, chrome- and vanadium-rich layers via hydrodynamic sorting of a mobilized cumulate slurry in a large, relatively slowly cooling, subsiding magma chamber. Miner. Depos. 48 : 1–56.

Mosier, D.L., Singer, D.A., Moring, B.C., and Galloway, J.P. (2012). Podiform chromite deposits—database and grade and tonnage models: U.S. Geological Survey Scientific Investigations Report 2012–5157, 45 p.

Mutanen, T. & Huhma, H. (2003). The 3.5 Ga Siurua trondhjemite gneiss in the Archean Pudasjärvi Granulite Belt, northern Finland. Bulletin of the Geological Society of Finland, 75, pp. 55-68.

Naldrett, A., Kinnaird, J., Wilson, A., Yudovskaya, M. & Chunnett, G. (2012). The origin of chromitites and related PGE mineralization in the Bushveld Complex: new mineralogical and petrological constraints. Mineralium Deposita 47, 209–232.

Namur, O., Abily, B., Boudreau, A., Blanchette, F., Bush, J. W. M., Ceuleneer, G., Charlier, B., Donaldson, C. H., Higgins, M. D., Morata, D., Nielsen, T. F. D., O'Driscoll, B., Pang K.-N., Peacock, T., Spandler, C., Toramaru, A. & Veksler, I. (2015). Igneous layering in basaltic magma chambers. In: Charlier, B., Namur, O., Latypov, R. & Tegner, C. (eds) Layered Intrusions, 1st edn. Springer, pp. 75–152.

Paulick, H., Bach, W., Godard, M., De Hoog, J. C. M., Suhr, G. and Harvey, J. (2006). Geochemistry of abyssal peridotites (Mid-Atlantic Ridge, 15_20'N, ODP Leg 209): Implications for fluid/rock interaction in slow spreading environments. Chemical Geology 234, 179–210.

Perttunen, V. & Vaasjoki, M. (2001). U–Pb geochronology of the Peräpohja Schist Belt,

northwestern Finland. Geological Survey of Finland, Special Paper 33, pp. 45-84.

Polovina, J. S., Hudson, D. M., and Jones, R. E. (2004). Petrographic and geochemical characteristics of postmagmatic hydrothermal alteration and mineralization in the J–J Reef, Stillwater Complex, Montana. The Canadian Mineralogist; 42 (2): 261–277. doi: https://doi.org/10.2113/gscanmin.42.2.261

Rouméjon, S., and Cannat, M. (2014). Serpentinization of mantle-derived peridotites at mid-ocean ridges: Mesh texture development in the context of tectonic exhumation, Geochem. Geophys. Geosyst., 15, 2354–2379, doi:10.1002/2013GC005148.

Rouméjon, S., Cannat, M., Agrinier, P., Godard, M., and Andreani, M. (2015). Serpentinization and Fluid Pathways in Tectonically Exhumed Peridotites from the Southwest Indian Ridge (62–65°E), Journal of Petrology, Volume 56, Issue 4, 1 April 2015, Pages 703–734, https://doi.org/10.1093/petrology/egv014

Scoon, R. N., & Mitchell, A. A. (2012). The Upper Zone of the Bushveld Complex at Roossenekal, South Africa: Geochemical stratigraphy and evidence of multiple episodes of magma replenishment. South African Journal of Geology. 115 (4): 515–534

Sen, G. (2014). Petrology, principles and practice. Springer, 370 pp.

Vaasjoki, M., Korsman, K., Koistinen, T. (2005). Overview. In: Lehtinen, M., Nurmi, P.A., Rämö, O.T. (Eds.), The Precambrian Geology of Finland – Key to the Evolution of the Fennoscandian Shield. Elsevier B.V., Amsterdam, pp. 1–18.

Vasilopanagos, C. (2016). Magma replenishment in the Kemi intrusion: evidence from silicate mineral chemistry. M.Sc., thesis, University of Oulu. p. 55.

Wicks, F. J. & Whittaker, E. J. W. (1977). Serpentine textures and serpentinization. Can Mineral 15:459–488.

Wicks, F. J. & O'Hanley, D. S. (1988). Serpentine minerals: structure and petrology. In: Bailey SW (Ed) Hydrous Phyllosilicates (other than mica). Reviews in Mineralogy, 19, Mineralogical Society of America, Washington, DC, pp. 91–168.

Yang, S.-H., Hanski, E., Li, C., Maier, W. D., Huhma, H., Mokrushin, A. V., Latypov, R., Lahaye, Y., O'Brian, H., Qu, W.-J. (2016). Mantle source of the 2.44-2.50-Ga mantle plume-related magmatism in the Fennoscandian Shield: evidence from Os, Nd, and Sr

isotope compositions of the Monchepluton and Kemi intrusions. Mineralium Deposita, DOI 10.1007/s00126-016-0673-9.

Appendix 1. Abbreviations used in Grönholm (1994) petrography.

Mineral	Abbreviation
Chlorite	Chl
Carbonate	Crb
Magnetite	Mag
Phlogopite	Phl
Pyroxene	Px
Serpentine	Srp
Talc	Tlc
Tremolite	Tr

Appendix 2. Modal composition of cumulate peridotites. From Grönholm (1994). Composition of the Alteration products (px) are mentioned in order of decreasing abundance next to the thin section's name.

Mineral/Minerals	1	2
Olivine	10.8	9.9
Clinopyroxene	23.1	26.8
Orthopyroxene	20.8	0.0
Amphibole	5.5	5.2
Chlorite	8.5	11.5
Serpentine	20.4	30.9
Phlogopite	0.3	0.0
Talc	0.0	0.0
Magnetite	5.3	6.6
Chromite	1.3	0.4
Alteration products (Px)	4	8.7
Pyrite	0.0	0.0

1 ELI-67-9.30-9.40; Srp, Tlc, Crb, Phl.

2 ELI-83-47,70; Srp, Tr.

Appendix 3. Modal composition of chlorite peridotites. From Grönholm (1994). Composition of the Alteration products (px) are mentioned in order of decreasing abundance next to the thin section's name.

Mineral/Minerals	1	2	3	4	5	6	7
Olivine	0.0	0.0	0.0	0.0	0.0	6.4	4.3
Pyroxene	0.0	0.5	0.0	2.6	6.6	0.5	0.7
Serpentine	52.9	41.8	51.5	53.2	43.9	57.3	42.9
Chlorite	14.9	18.6	20.2	20.3	17.7	16.6	22.6
Amphibole	2.5	11.6	7.6	9.5	0.0	0.0	15.1
Phlogopite	0.0	0.0	0.0	0.1	0.1	0.3	2.1
Carbonate	7.9	9.4	11.1	4.3	0.0	0.3	0.0
Alteration products (Px)	14.3	10.7	5.6	2.0	18.5	0.0	7.5
Magnetite	7.5	5.7	0.8	6.5	11.4	9.9	3.6
Chromite	0.0	1.7	3.2	1.5	1.8	8.7	1.2
Pyrite	0.1	0.1	0.1	0.1	0.1	0.1	0.1
Phyrrhotite	0.0	0.0	0.1	0.0	0.0	0.0	0.1
Chalcopyrite	0.0	0.0	0.1	0.0	0.0	0.0	0.0

1 R25-65.75; Tr, Mag, Srp, Crb.
2 ELI-675-15.00; Srp, Tr, Mag.
3 ELI-674-26.25; Tr, Srp, Mag, Crb.
4 ELI-671-13.5; Tr, Srp, Mag.
5 ELI-674-15.75; Tr, Srp.
6 R25 -23.50.
7 ELI-673-8.50; Tr, Srp, Mag.

Appendix 4. Modal composition of serpentine peridotites. From Grönholm (1994). Composition of the Alteration products (px) are mentioned in order of decreasing abundance next to the thin section's name.

Mineral/Minerals	1	2	3	4	5	6	7	8	9	10
Olivine	0	0	0.1	0	0	0	0	0	4.5	0
Pyroxene	0	0	3.7	4.6	0	0	0.2	0	9.1	1.7
Serpentine	56.7	68.4	68	64	60.8	61.2	59.7	56.2	58.3	60.4
Chlorite	13.7	11	4.7	8.1	6.6	14.2	11.1	10.9	9	17.3
Amphibole	3.5	0.1	0	0.4	9.4	9.9	2.8	1.4	0.8	9.2
Phlogopite	0	0	4.8	2.3	0	0	1.1	0.1	4.7	0.9
Carbonate	8.4	9.5	0	3	7.7	8.4	3.4	11.2	0	0.6
Alteration products (Px)	14.5	8.5	0.6	0	0	0	19	18.5	0	0
Magnetite	2.5	0	17.2	16.3	0	4.3	1.3	0.4	13.5	9.9
Chromite	0.7	2.5	0.9	1.3	15.5	2	1.4	1.3	0.1	0
Pyrite	0.1	0	0.1	0.1	0.1	0.1	0.1	0.1	0.1	0.1
Pyrrhotite	0	0	0	0	0	0.1	0	0	0	0

1 ELI-670-6,00; Tr, Tlc, Mag, Srp, Crb
2 ELI-211-142;15, Tr, Srp, Mag, Crb
3 R22-72
4 ELI-671-8
5 ELI-674-36,30
6 ELI-675-4,75
7 ELI-670-15,50; Mag, Tr, Srp, Crb, Tlc
8 ELI-675-27.50; Tr, Tlc, Srp, Mag
9 ELI-672-16,90
10 ELI-195-33,10

Appendix 5. Modal composition of amphibole peridotites. From Grönholm (1994). Composition of the Alteration products (px) are mentioned in order of decreasing abundance next to the thin section's name.

Mineral/Minerals	1	2	3	4
Pyroxene	0	0.2	0	0
Serpentine	41.8	36.5	49	46
Chlorite	18.8	25.8	16.9	6.4
Amphibole	20.3	22.5	14.8	28.4
Phlogopite	0.1	0.1	0.9	0
Carbonate	3.5	0.6	1.5	2
Alteration products (Px)	13.3	13.4	14.6	0
Magnetite	0	0	0	0.4
Chromite	2.2	0.9	2.3	16.8
Pyrite	0.1	0.1	0.1	0

1 ELI-675-21,00; Tr, Chl, Mag
2 ELI-672-24,50; Mag, Srp, Tr, Chl
3 ELI-673-71,4; Tr, Mag, Srp, Crb
4 ELI-672-28,80

Appendix 6. Modal composition of pyroxene peridotites. From Grönholm (1994). Composition of the Alteration products (px) are mentioned in order of decreasing abundance next to the thin section's name.

Mineral/ Minerals	1	2	3	4	5	6	7	8	9	10	11	12	13	14	15
Olivine	0	0	0	0	0	1.9	0	0	0	0	0	0	0	0	0
Pyroxene	9.1	0	0	0	2	6.2	2.4	0	0	0	0	0	0	0.5	0.2
Serpentine	55.1	58.1	43.1	44.9	37.7	32	53.1	51.7	51.1	56.9	51.8	38.8	41.1	31.1	46.4
Chlorite	8.3	0.7	14.6	5.9	4.5	8.6	14.5	12.3	11	7.6	15.2	8.2	17	16.2	12.2
Phlogopite	8.8	1	0.1	0.6	0.6	0.5	0	0.3	0.2	3.2	0	0	0	0	0
Carbonate	3.1	0.4	0	2.2	1.4	0.1	0.1	4.9	6.4	0.6	7.4	7.9	0.4	4.1	11.4
Amphibole	6.9	0	4.4	2.5	3.6	5.9	0.1	11.7	5.2	1.9	1.1	7	9.6	36.7	15.5
Talc	0	0	0	0	0	0	0	0	0	0	0	0	0	0	3.9
Alteration products (Px)	0	32.8	35.5	42.7	45	41.3	0.3	18.2	19.5	28.2	20.7	30	31.2	0	0
Magnetite	5.7	2.5	0	0	0	2.2	26.6	0.8	0.6	0.3	0	0	0	0.7	0.1
Chromite	3	4.5	2.3	1.2	5.2	1.3	2.9	0.1	6	1.3	3.8	8.1	0	10.7	10.4
Pyrrhotite	0	0	0	0	0	0	0	0	0.1	0	0	0	0	0	0.1
Pyrite	0	0.1	0	0	0	0.1	0.1	0.1	0.1	0.1	0.1	0.1	0.1	0.1	0.1

1 ELI-47-20.57
2 R22-47,0; Tr, Crb, TIc, ChI, Srp, Mag
3 ELI-675-54.1; Tlc, Tr, Srp, Chl
4 R22-109: Tr, Crb, Mag, Srp
5 R22-98; Mag, Tr, Srp, Chl
6 ELI-672-5,7; Mag, Tr, Srp, Chl
7 R22-87, Mag
8 ELl-671-25.7; Tr, Chl, Srp, Crb, Mag
9 ELI-670-23; Tlc, Srp, Tr, Crb, Mag
10 ELl-675-63, Tr, Mag, Crb, Tlc, Srp, Chl
11 R22-119,50, Crb, Tr, Tlc, Srp, Chl, Mag
12 ELl-673-20,10, Chl, Srp, Crb, Tr, Mag
13 ELl-673-61,00, Tr, Tlc, Srp, Chl
14 ELl-674-77,40
15 ELl-670-43,50

Appendix 7. Modal composition of amphibole pyroxenites. From Grönholm (1994). Composition of the Alteration products (px) are mentioned in order of decreasing abundance next to the thin section's name.

Mineral/Minerals	1	2	3	4	5	6	7
Pyroxene	30.4	0	42.6	57.4	7.4	14.7	0
Amphibole	29.4	70.5	30.6	28.7	60.7	44.8	76.6
Chlorite	24	27.5	21.1	12.4	16.5	32.6	11.5
Serpentine	3.1	1.2	0	0	0	0.1	3.6
Phlogopite	0.1	0	0	0.1	0	0	0
Talc	4.9	0	3.7	1.2	15.4	6.9	0
Alteration products (Px)	7.9	0	0	0	0	0	0
Carbonate	0.1	0	0	0	0	0	2.8
Magnetite	0.1	0.8	2	0.2	0	0.9	5.5
Chromite	0.1	0.1	0	0	0	0.1	0.1
Pyrrhotite	0	0	0	0	0.1	0	0.1
Pyrite	0	0.1	0.1	0	0	0.1	0.1

1 ELI-670-52.50 Fine-grained material after Px
2 R22-56.00
3 ELI-674-73.00
4 ELI-672-45.60
5 ELI-672-34.00
6 ELI-672-30.80
7 ELI-674-65.70

Appendix 8. Modal composition of talc pyroxenites. From Grönholm (1994). Composition of the Alteration products (px) are mentioned in order of decreasing abundance next to the thin section's name.

Mineral/Minerals	1	2
Pyroxene	1.5	1.5
Amphibole	27.4	15.8
Chlorite	35.4	18
Talc	33.2	50
Serpentine	0.6	1.4
Phlogopite	0.3	1.2
Plagioclase	0	0
Alteration products (Px)	0	9.7
Magnetite	1.6	2.4
Chromite	0.1	0
Pyrite	0.1	0.1

1 R25-57.00

2 R25-27.00; Srp, Tr

Appendix 9. Modal composition of serpentinites. From Grönholm (1994).

Mineral/Minerals	1	2	3	4	5
Serpentine	90.2	75.7	71.3	78.6	81.8
Chlorite	0	0	9.7	0	0.1
Carbonate	1.2	10.1	0	0	3.4
Talc	0	2.1	0	0	8.9
Magnetite	8.6	10	16.9	18.9	0
Chromite	0	2.1	2.1	2.5	5.8

1 ELI-550-38.55
2 ELI-512-34.80
3 ELI-51-140.39
4 ELI-731-147.45
5 ELI-SP-2

Appendix 10. Microprobe analysis results in chromitites.

Na2O	CaO	Cr2O3	P2O5	MgO	FeO	MnO	K2O	Al2O3	NiO	TiO2	SiO2	Total	Sample-Point	Mineral
0.00	0.00	47.99	0.00	6.12	29.80	0.39	0.00	13.88	0.10	0.56	0.00	98.85	ELI-453-42.10-1	Chromite
0.00	0.00	56.10	0.01	5.81	26.66	0.36	0.00	11.57	0.02	0.48	0.03	101.04	ELI-453-42.10-2	Chromite rim
0.16	0.21	2.08	0.00	23.35	1.43	0.00	9.80	14.58	0.25	3.34	39.10	94.29	ELI-453-42.10-3	Phlogopite
0.20	0.00	2.54	0.00	23.72	1.26	0.00	10.30	15.01	0.25	0.89	40.29	94.46	ELI-453-42.10-4	Phlogopite
0.26	13.28	0.72	0.00	23.30	1.11	0.04	0.04	1.44	0.08	0.01	57.03	97.31	ELI-453-42.10-5	Amphibole
0.02	0.00	48.69	0.00	6.43	28.61	0.36	0.01	14.42	0.08	0.75	0.02	99.39	ELI-453-42.10-6	Chromite
0.09	0.05	56.65	0.00	5.56	26.14	0.43	0.05	9.91	0.04	0.17	0.86	99.96	ELI-453-42.10-7	Chromite rim
0.06	0.03	0.04	0.00	30.87	0.60	0.00	0.01	0.04	0.12	0.01	62.24	94.02	ELI-453-42.10-8	Talc
0.20	0.00	2.52	0.00	24.68	1.20	0.01	10.24	14.40	0.20	0.43	40.92	94.79	ELI-453-42.10-9	Phlogopite

Appendix 11. Microprobe analysis results in cumulate peridotites.

Na2O	CaO	Cr2O3	P2O5	MgO	FeO	MnO	K2O	Al2O3	NiO	TiO2	SiO2	Total	Sample-Point	Mineral
0.00	0.00	30.63	0.00	1.90	47.99	0.62	0.01	11.64	0.11	4.30	0.00	97.20	ELI-67-9.30-9.40 1	Chromite
0.27	0.56	0.00	0.02	30.18	5.45	0.36	0.07	12.86	0.04	0.07	34.74	84.60	ELI-67-9.30-9.40 2	Chlorite
0.34	11.32	0.17	0.01	23.07	4.37	0.15	0.03	0.90	0.04	0.06	56.20	96.65	ELI-67-9.30-9.40 3	Amphibole
0.00	0.61	0.00	0.00	25.99	17.28	0.31	0.07	0.04	0.03	0.04	38.55	82.92	ELI-67-9.30-9.40 4	Serpentine
0.01	0.06	0.00	0.00	44.68	15.77	0.19	0.01	0.01	0.17	0.01	40.40	101.31	ELI-67-9.30-9.40 5	Olivine
0.10	0.00	30.96	0.00	2.10	49.32	0.69	0.00	11.68	0.13	3.55	0.03	98.56	ELI-67-9.30-9.40 7	Chromite
0.07	0.04	0.02	0.04	44.89	16.61	0.26	0.02	0.00	0.19	0.02	40.46	102.60	ELI-67-9.30-9.40 6	Olivine
1.01	0.00	1.52	0.00	23.37	6.18	0.06	7.07	15.11	0.07	3.28	37.80	95.47	ELI-67-9.30-9.40 8	Phlogopite
0.22	0.73	0.00	0.00	28.42	7.05	0.10	0.07	15.53	0.07	0.03	33.37	85.58	ELI-67-9.30-9.40 9	Chlorite
0.86	13.59	1.14	0.03	21.26	3.27	0.04	0.02	3.01	0.05	0.15	55.25	98.67	ELI-67-9.30-9.40 10	Amphibole
0.06	0.00	38.86	0.00	8.81	32.92	0.35	0.00	16.58	0.09	1.11	0.02	98.79	ELI-83-477-47.8 1	Chromite
0.06	0.10	0.01	0.00	34.01	5.88	0.16	0.04	5.11	0.00	0.02	38.36	83.75	ELI-83-477-47.8 2	Serpentine
0.19	12.14	0.00	0.02	22.80	3.60	0.15	0.02	0.63	0.04	0.01	56.10	95.69	ELI-83-477-47.8 3	Amphibole
0.04	0.34	0.00	0.00	25.90	15.75	0.31	0.03	0.20	0.00	0.03	37.97	80.57	ELI-83-477-47.8 4	Serpentine
0.49	0.77	0.00	0.00	25.89	6.94	0.07	0.34	19.19	0.07	0.04	31.09	84.89	ELI-83-477-47.8 5	Chlorite
0.47	0.48	0.00	0.04	26.76	7.97	0.17	0.74	18.03	0.05	0.03	31.68	86.42	ELI-83-477-47.8 6	Chlorite
0.18	12.97	0.02	0.00	22.97	3.05	0.09	0.03	0.24	0.02	0.00	58.04	97.61	ELI-83-477-47.8 7	Amphibole
0.13	0.48	0.02	0.01	28.50	14.19	0.28	0.07	0.48	0.02	0.00	37.61	81.79	ELI-83-477-47.8 8	Serpentine
0.05	0.10	0.00	0.03	44.95	15.83	0.27	0.03	0.02	0.18	0.00	40.93	102.38	ELI-83-477-47.8 9	Olivine

Appendix 12. Microprobe analysis results in chlorite peridotites.

Na2O	CaO	Cr2O3	P2O5	MgO	FeO	MnO	K2O	Al2O3	NiO	TiO2	SiO2	Total	Sample-Point	
0.17	22.43	0.37	0.03	17.63	3.73	0.06	0.04	0.18	0.02	0.06	53.74	98.43	ELI-671-13.50 1	Clinopyroxene
0.66	22.97	1.14	0.04	15.74	3.96	0.12	0.04	3.41	0.02	0.29	52.58	100.98	ELI-671-13.50 2	Clinopyroxene
0.01	0.02	0.00	0.00	33.33	8.16	0.17	0.00	2.63	0.12	0.01	42.06	86.50	ELI-671-13.50 3	Serpentine
0.30	0.03	33.47	0.00	8.52	34.49	0.34	0.10	15.83	0.08	2.03	0.07	95.26	ELI-671-13.50 4	Chromite
0.00	52.60	0.00	0.00	2.65	0.64	0.34	0.00	0.33	0.01	0.01	1.03	57.61	ELI-671-13.50 5	Calcite
0.11	0.02	0.00	0.02	30.63	7.29	0.10	0.17	12.89	0.12	0.01	34.11	85.48	ELI-671-13.50 6	Chlorite
0.00	54.95	0.00	0.04	1.73	0.54	0.31	0.00	0.37	0.00	0.01	0.26	58.20	ELI-671-13.50 7	Calcite
0.00	0.01	0.00	0.00	31.21	6.94	0.09	0.12	13.60	0.11	0.03	34.22	86.32	ELI-671-13.50 8	Chlorite
0.01	0.00	0.01	0.00	30.71	7.57	0.05	0.10	13.75	0.17	0.03	34.10	86.50	ELI-671-13.50 9	Chlorite
0.00	0.00	0.01	0.03	33.66	7.38	0.20	0.01	1.42	0.09	0.01	42.88	85.68	ELI-671-13.50 10	Serpentine
0.00	0.00	34.81	0.00	2.54	41.11	1.76	0.00	15.65	0.09	1.77	0.00	97.71	ELI-671-13.50 11	Chromite rim
0.06	29.53	0.01	0.02	18.03	3.95	0.71	0.01	0.00	0.01	0.00	0.00	52.32	ELI-674-26.25 1	Dolomite
1.20	0.04	36.10	0.01	8.01	31.93	0.41	0.30	17.53	0.08	1.04	0.07	96.73	ELI-674-26.25 2	Chromite
0.08	0.00	0.02	0.00	32.24	10.05	0.10	0.02	3.19	0.08	0.03	41.22	87.03	ELI-674-26.25 3	Serpentine
0.14	0.00	37.01	0.06	7.83	34.31	0.48	0.00	16.09	0.09	1.56	0.00	97.57	ELI-674-26.25 4	Chromite
0.04	0.01	0.11	0.00	29.72	9.11	0.05	0.09	12.99	0.09	0.03	34.16	86.41	ELI-674-26.25 5	Chlorite
0.26	13.74	0.00	0.02	22.38	2.40	0.14	0.07	0.33	0.08	0.02	57.65	97.08	ELI-674-26.25 6	Amphibole
0.01	0.00	35.90	0.02	5.12	38.17	0.75	0.01	16.63	0.07	1.21	0.00	97.90	ELI-674-26.25 7	Chromite rim
0.06	28.76	0.01	0.02	18.09	3.66	0.74	0.01	0.47	0.00	0.00	0.89	52.69	ELI-674-26.25 8	Dolomite
0.03	0.04	0.04	0.00	33.26	9.51	0.08	0.00	1.31	0.10	0.02	42.32	86.70	ELI-674-26.25 9	Serpentine
0.03	0.00	33.43	0.02	0.22	58.37	1.33	0.00	1.23	0.06	1.66	0.10	96.44	ELI-674-26.25 10	Chromite
0.54	12.83	1.03	0.04	21.52	4.58	0.16	0.03	0.99	0.04	0.04	57.34	99.15	ELI-674-26.25 11	Clinopyroxene
0.05	0.01	37.74	0.00	7.62	33.41	0.38	0.00	16.16	0.12	2.11	0.00	97.62	R25-5-65.75 1	Chromite
0.01	29.36	0.00	0.01	17.99	3.72	0.62	0.00	0.00	0.00	0.03	0.00	51.74	R25-5-65.75 2	Dolomite
0.00	58.57	0.00	0.01	0.26	0.06	0.51	0.00	0.00	0.08	0.00	0.00	59.49	R25-5-65.75 3	Calcite
0.07	13.50	0.00	0.05	22.07	3.64	0.17	0.02	0.06	0.07	0.02	58.97	98.63	R25-5-65.75 4	Amphibole
0.00	0.00	0.00	0.02	32.95	9.65	0.09	0.00	0.92	0.14	0.02	42.51	86.29	R25-5-65.75 5	Serpentine
0.62	13.11	0.95	0.00	21.22	4.57	0.19	0.06	1.30	0.05	0.07	57.25	99.40	R25-5-65.75 6	Clinopyroxene
0.01	0.05	1.04	0.03	32.55	9.66	0.10	0.01	3.09	0.09	0.01	41.15	87.78	R25-5-65.75 6.5	Serpentine
0.04	0.00	43.35	0.00	9.00	30.48	0.39	0.01	15.41	0.09	0.50	0.00	99.27	R25-5-65.75 7	Chromite
0.03	0.00	38.57	0.01	8.44	33.04	0.41	0.01	16.25	0.10	1.65	0.00	98.49	R25-5-65.75 8	Chromite
0.01	0.02	0.03	0.00	30.50	8.23	0.06	0.03	14.04	0.17	0.02	33.45	86.55	R25-5-65.75 9	Chlorite
0.00	0.00	35.70	0.00	5.26	37.44	0.62	0.00	16.28	0.08	2.30	0.00	97.67	R25-5-65.75 10	Chromite
0.00	19.66	0.05	0.01	23.39	5.57	0.42	0.00	1.03	0.04	0.01	14.02	64.19	R25-5-65.75 11	Dolomite

0.10	0.00	35.71	0.01	7.00	36.83	0.43	0.03	15.47	0.05	2.27	0.00	97.87	R25-23.5-001	Chromite
0.19	0.00	18.59	0.00	0.66	69.45	2.49	0.02	1.20	0.06	1.36	0.08	94.10	R25-23.5-2	Chromite rim
0.00	0.04	0.00	0.01	35.66	2.95	0.10	0.02	0.00	0.17	0.00	48.57	87.52	R25-23.5-3	Serpentine
0.00	0.31	0.05	0.00	25.80	10.47	0.17	0.08	0.02	0.00	0.01	47.67	84.58	R25-23.5-4	Serpentine
0.09	0.49	0.00	0.00	23.31	14.94	0.35	0.04	0.02	0.01	0.03	41.48	80.75	R25-23.5-5	Serpentine
0.03	0.00	35.17	0.03	0.00	39.96	0.58	0.02	0.00	0.33	2.62	0.01	78.75	R25-23.5-6	Chromite
0.01	0.00	0.54	0.01	0.00	90.55	0.08	0.00	0.01	0.31	0.20	0.01	91.71	R25-23.5-7	Chromite rim
0.03	0.09	0.21	0.03	46.33	14.54	0.18	0.00	0.00	0.10	0.05	39.71	101.27	R25-23.5-9	Olivine
0.03	0.13	0.10	0.02	27.71	12.76	0.15	0.08	0.00	0.00	0.02	44.34	85.34	R25-23.5-10	Serpentine
0.01	0.00	0.07	0.00	38.94	3.05	0.07	0.02	0.38	0.00	0.00	43.78	86.31	R25-23.5-11	Serpentine
0.00	0.42	0.27	0.00	23.40	15.55	0.05	0.04	0.00	0.00	0.01	46.27	86.01	R25-23.5-12	Serpentine

Appendix 13. Microprobe analysis results in serpentine peridotites.

Na2O	CaO	Cr2O3	P2O5	MgO	FeO	MnO	K2O	Al2O3	NiO	TiO2	SiO2	Total	Sample-Point	Mineral
0.03	26.43	0.07	0.00	17.77	2.20	0.05	0.00	0.00	0.02	0.00	56.29	102.87	R22.2-72 1	Clinopyroxene
0.03	0.02	1.01	0.01	27.74	5.66	0.23	3.84	13.63	0.08	1.27	33.75	87.26	R22.2-72 2	Phlogopite
0.01	0.00	0.02	0.00	35.34	5.60	0.15	0.03	2.03	0.06	0.01	42.49	85.74	R22.2-72 3	Serpentine
0.54	23.31	0.93	0.00	16.12	4.53	0.13	0.01	2.91	0.01	0.33	53.24	102.06	R22.2-72 4	Clinopyroxene
0.01	0.66	0.03	0.00	21.77	22.27	0.22	0.05	0.03	0.19	0.03	41.98	87.23	R22.2-72 5	Serpentine
0.00	0.00	28.00	0.00	2.13	51.73	0.99	0.01	11.40	0.14	4.12	0.03	98.54	R22.2-72 6	Chromite
0.02	0.00	31.24	0.00	3.30	46.28	0.78	0.00	11.49	0.14	3.52	0.06	96.83	R22.2-72 7	Chromite
0.00	0.00	0.00	0.00	36.02	5.42	0.13	0.00	1.64	0.08	0.00	43.19	86.48	R22.2-72 8	Serpentine
0.00	54.35	0.00	41.56	0.40	0.25	0.01	0.01	0.00	0.02	0.01	0.03	96.63	ELI-670-15.50 1	Apatite
0.39	13.22	0.10	0.00	22.15	3.12	0.10	0.02	0.60	0.04	0.05	57.85	97.63	ELI-670-15.50 2	Amphibole
0.09	0.00	36.03	0.00	3.63	43.77	0.86	0.00	12.27	0.10	1.77	0.02	98.54	ELI-670-15.50 3	Chromite
0.00	0.00	0.30	0.00	0.01	91.50	0.04	0.00	0.01	0.03	0.24	0.02	92.15	ELI-670-15.50 3.5	Chromite rim
0.04	0.00	1.24	0.00	29.46	8.72	0.06	0.33	13.06	0.13	0.70	32.67	86.42	ELI-670-15.50 4	Chlorite
0.00	30.09	0.00	0.02	18.62	2.30	0.58	0.02	0.01	0.00	0.03	0.00	51.66	ELI-670-15.50 5	Dolomite
0.15	0.00	33.10	0.04	1.37	47.97	1.20	0.00	13.46	0.17	2.92	0.00	100.39	ELI-670-15.50 6	Chromite
0.00	0.00	0.01	0.04	33.03	9.03	0.12	0.01	1.01	0.09	0.01	42.31	85.65	ELI-670-15.50 7	Serpentine
0.20	12.31	0.00	0.01	23.42	3.27	0.14	0.04	0.65	0.05	0.02	56.39	96.51	ELI-670-15.50 8	Amphibole
0.05	0.00	33.19	0.00	7.34	38.20	0.41	0.03	14.08	0.10	2.49	0.02	95.90	ELI-670-15.50 9	Chromite
0.04	0.00	42.91	0.01	9.54	27.93	0.45	0.00	17.23	0.05	0.56	0.02	98.73	ELI-674-36.30 1	Chromite
0.23	12.85	0.13	0.00	22.60	2.49	0.15	0.03	0.26	0.04	0.02	57.54	96.35	ELI-674-36.30 2	Amphibole
0.00	0.17	1.01	0.00	31.92	9.04	0.04	0.01	2.79	0.12	0.00	41.16	86.26	ELI-674-36.30 3	Serpentine
0.35	0.01	37.93	0.00	8.58	30.68	0.44	0.08	18.77	0.11	1.47	0.03	98.46	ELI-674-36.30 4	Chromite
0.00	0.07	0.32	0.00	31.42	8.99	0.10	0.03	3.01	0.11	0.00	40.71	84.75	ELI-674-36.30 5	Serpentine
0.00	0.04	0.06	0.02	32.92	9.22	0.10	0.00	1.25	0.11	0.02	42.44	86.17	ELI-674-36.30 6	Serpentine
0.00	0.01	0.07	0.03	33.25	7.80	0.08	0.00	1.03	0.09	0.00	42.31	84.67	ELI-674-36.30 7	Serpentine
0.97	12.70	1.17	0.01	22.54	3.57	0.20	0.02	1.90	0.02	0.06	56.16	99.32	ELI-674-36.30 8	Amphibole
0.06	2.09	0.90	0.00	32.04	8.17	0.08	0.01	2.42	0.10	0.03	44.63	90.53	ELI-674-36.30 9	Chl/Amp
0.00	0.02	42.81	0.00	9.57	27.18	0.39	0.01	16.75	0.06	0.49	0.07	97.34	ELI-674-36.30 10	Chromite
0.07	0.08	0.24	0.02	31.68	9.45	0.06	0.02	5.63	0.12	0.02	39.08	86.47	ELI-675-27.50 1	Serpentine
0.06	0.10	0.07	0.03	32.55	9.09	0.10	0.04	2.30	0.09	0.02	41.60	86.05	ELI-675-27.50 2	Talc
0.00	0.14	0.25	0.00	31.43	9.53	0.08	0.01	6.84	0.08	0.01	38.84	87.20	ELI-675-27.50 3	Talc
0.00	0.02	0.10	0.03	32.04	9.38	0.06	0.00	2.98	0.07	0.00	41.27	85.94	ELI-675-27.50 4	Talc
0.30	11.94	0.38	0.01	22.83	3.21	0.08	0.06	1.33	0.02	0.05	56.58	96.79	ELI-675-27.50 5	Amphibole
0.53	12.94	0.77	0.00	22.18	3.80	0.14	0.04	1.20	0.03	0.02	56.87	98.53	ELI-675-27.50 6	Amphibole
0.01	0.00	1.14	0.00	29.13	8.80	0.09	0.25	13.29	0.12	0.15	33.17	86.15	ELI-675-27.50 7	Chlorite
0.01	0.02	0.00	0.00	32.93	8.93	0.12	0.01	1.55	0.07	0.00	42.19	85.82	ELI-675-27.50 8	Serpentine
0.06	0.00	38.45	0.02	9.18	29.66	0.40	0.01	18.38	0.11	1.23	0.00	97.50	ELI-675-27.50 9	Chromite
0.00	0.00	31.12	0.00	1.21	47.16	1.05	0.01	13.62	0.12	3.88	0.01	98.17	ELI-675-27.50 10	Chromite

Appendix 14. Microprobe analysis results in amphibole peridotites.

Na2O	CaO	Cr2O3	P2O5	MgO	FeO	MnO	K2O	Al2O3	NiO	TiO2	SiO2	Total	Sample-Point	Mineral
0.44	12.79	0.01	0.00	21.60	4.60	0.22	0.05	0.71	0.03	0.01	57.36	97.79	ELI-675-21.00 1	Amphibole
0.01	0.00	0.02	0.01	33.44	10.20	0.08	0.01	0.63	0.07	0.02	43.40	87.87	ELI-675-21.00 2	Serpentine
0.01	0.03	0.16	0.00	29.01	9.82	0.05	0.01	11.67	0.08	0.00	34.40	85.22	ELI-675-21.00 3	Chlorite
0.01	0.03	0.11	0.00	31.31	11.09	0.09	0.01	2.23	0.06	0.00	41.86	86.79	ELI-675-21.00 4	Serpentine
0.00	0.03	0.04	0.01	31.03	10.09	0.06	0.01	10.64	0.07	0.03	35.79	87.80	ELI-675-21.00 5	Chlorite
0.00	0.00	31.50	0.00	1.30	49.76	1.08	0.00	12.16	0.15	2.84	0.00	98.79	ELI-675-21.00 6	Chromite
0.00	0.00	30.13	0.00	0.20	64.26	0.92	0.00	1.78	0.07	1.71	0.00	99.07	ELI-675-21.00 6.5	Chromite rim
0.01	0.00	0.02	0.00	28.23	10.82	0.05	0.00	15.99	0.08	0.03	31.39	86.62	ELI-675-21.00 7	Chlorite
0.01	0.09	1.02	0.00	29.44	9.45	0.04	0.00	10.23	0.10	0.04	34.08	84.48	ELI-675-21.00 8	Chlorite
0.26	13.73	0.25	0.00	22.24	3.85	0.21	0.00	0.50	0.05	0.03	59.06	100.17	ELI-675-21.00 9	Diopside
0.28	13.47	0.07	0.02	21.96	3.88	0.11	0.01	0.30	0.05	0.01	58.08	98.23	ELI-675-21.00 10	Amphibole
0.16	13.55	0.07	0.02	21.19	4.39	0.11	0.02	0.29	0.06	0.00	57.46	97.30	ELI-675-21.00 11	Amphibole
0.00	0.00	0.01	0.01	33.20	9.26	0.10	0.00	0.95	0.09	0.02	43.14	86.78	ELI-673-71.40 1	Serpentine
0.00	34.79	0.01	0.06	11.84	3.69	0.24	0.00	0.80	0.01	0.00	12.32	63.75	ELI-673-71.40 2	Dol/Srp
0.21	13.30	0.02	0.01	22.42	3.07	0.09	0.01	0.21	0.05	0.02	58.17	97.55	ELI-673-71.40 3	Amphibole
0.01	0.00	35.62	0.02	2.29	41.46	0.85	0.03	14.36	0.13	2.25	0.00	97.02	ELI-673-71.40 4	Chromite
0.01	0.09	31.76	0.00	0.27	58.75	1.11	0.00	0.47	0.06	1.46	0.16	94.14	ELI-673-71.40 5	Chromite rim
0.00	0.00	0.09	0.00	29.90	9.92	0.02	0.07	12.37	0.09	0.02	34.87	87.35	ELI-673-71.40 6	Chlorite
0.02	26.86	0.04	0.03	14.74	5.46	0.25	0.01	2.27	0.07	0.00	15.69	65.43	ELI-673-71.40 7	Dol/Chl
0.36	12.59	0.62	0.00	22.18	4.60	0.15	0.01	0.62	0.04	0.03	57.04	98.25	ELI-673-71.40 8	Amphibole
0.08	0.00	36.34	0.00	2.62	38.72	0.85	0.00	17.30	0.05	1.34	0.00	97.30	ELI-673-71.40 9	Chromite
0.00	0.00	28.30	0.00	0.16	64.94	0.94	0.01	0.26	0.02	1.12	0.14	95.89	ELI-673-71.40 9.5	Chromite rim
0.29	13.24	0.01	0.00	22.53	2.93	0.14	0.01	0.35	0.06	0.00	59.33	98.89	ELI-673-71.40 10	Amphibole

Appendix 15. Microprobe analysis results in pyroxene peridotites.

Na2O	CaO	Cr2O3	P2O5	MgO	FeO	MnO	K2O	Al2O3	NiO	TiO2	SiO2	Total	Sample-Point	Mineral
0.03	0.00	37.23	0.00	9.76	31.22	0.37	0.03	18.80	0.09	0.57	0.01	98.11	R22-3-87 1	Chromite
0.00	0.01	37.27	0.02	9.44	31.09	0.43	0.00	18.97	0.07	0.55	0.00	97.84	R22-3-87 1.5	Chromite rim
0.36	18.44	1.08	0.00	14.58	16.91	0.15	0.01	1.91	0.03	0.24	44.28	97.99	R22-3-87 2	Clinopyroxene
0.50	20.46	1.11	0.04	16.66	4.44	0.10	0.01	3.69	0.00	0.23	50.83	98.06	R22-3-87 3	Clinopyroxene
0.01	0.00	0.00	0.00	30.88	5.09	0.07	0.01	14.91	0.11	0.01	32.64	83.73	R22-3-87 4	Chlorite
0.02	0.01	0.00	0.00	32.06	5.66	0.05	0.16	12.37	0.14	0.01	34.63	85.11	R22-3-87 5	Chlorite
0.05	0.00	0.01	0.00	35.71	5.33	0.17	0.02	1.71	0.09	0.00	42.85	85.94	R22-3-87 6	Serpentine
0.00	0.00	32.07	0.00	2.22	45.97	1.45	0.00	12.82	0.11	3.47	0.01	98.11	R22-3-87 7	Chromite
0.01	0.00	0.85	0.00	0.50	89.08	0.04	0.00	0.03	0.12	0.30	0.49	91.41	R22-3-87 7.5	Chromite rim
0.51	22.90	0.86	0.03	16.05	4.18	0.08	0.00	2.91	0.01	0.83	52.57	100.92	R22-3-87 8	Clinopyroxene
0.00	0.08	1.35	0.00	0.13	87.82	0.07	0.02	0.03	0.09	0.19	0.25	90.01	R22-3-87 9	Magnetite
0.77	22.48	1.07	0.01	15.05	4.33	0.07	0.01	3.65	0.03	0.32	51.66	99.44	R22-3-87 10	Clinopyroxene
0.00	0.02	0.02	0.07	0.26	89.04	0.11	0.00	0.02	0.09	0.60	0.47	90.69	R22-3-87 11	Magnetite
0.00	0.02	0.03	0.00	33.11	8.13	0.25	0.00	1.15	0.09	0.02	42.46	85.26	ELI-47-20.57-70 1	Serpentine
0.00	0.00	31.83	0.00	2.21	48.13	1.06	0.01	10.03	0.14	4.05	0.02	97.48	ELI-47-20.57-70 2	Chromite
0.03	0.00	31.60	0.00	2.11	48.70	1.03	0.01	10.19	0.13	3.98	0.02	97.79	ELI-47-20.57-70 2.5	Chromite rim
0.03	43.21	0.00	0.01	6.94	1.91	0.46	0.01	0.23	0.03	0.00	6.30	59.14	ELI-47-20.57-70 3	Calcite
0.00	58.07	0.00	0.03	1.25	0.55	0.63	0.04	0.00	0.02	0.00	0.00	60.59	ELI-47-20.57-70 4	Calcite
0.19	0.02	1.27	0.01	21.55	9.02	0.27	7.34	13.51	0.11	4.12	34.99	92.39	ELI-47-20.57-70 5	Phlogopite
0.01	0.01	32.94	0.00	4.82	45.90	0.63	0.00	11.50	0.15	3.23	0.00	99.18	ELI-47-20.57-70 6	Chromite
0.98	0.00	0.55	0.00	0.04	88.63	0.00	0.12	0.03	0.05	0.33	0.02	90.75	ELI-47-20.57-70 6.5	Chromite rim
0.06	0.07	0.01	0.01	0.04	91.35	0.00	0.00	0.00	0.06	0.24	0.08	91.92	ELI-47-20.57-70 7	Magnetite
0.03	0.00	0.02	0.00	33.10	8.79	0.14	0.01	1.98	0.09	0.00	42.62	86.77	ELI-47-20.57-70 8	Serpentine
0.55	12.53	0.02	0.02	21.70	4.16	0.18	0.03	0.66	0.07	0.01	56.55	96.47	ELI-47-20.57-70 9	Amphibole
0.09	0.00	27.03	0.00	1.32	51.29	1.74	0.01	9.43	0.13	4.26	0.00	95.30	ELI-47-20.57-70 10	Chromite
0.80	12.57	0.28	0.00	22.01	3.33	0.13	0.08	0.94	0.05	0.06	57.05	97.30	ELI-47-20.57-70 11	Amphibole
0.34	0.03	1.04	0.01	22.80	11.79	0.56	5.55	12.41	0.06	7.40	32.35	94.36	ELI-47-20.57-70 12	Phlogopite
0.07	0.02	0.00	0.01	31.36	7.87	0.08	0.25	11.27	0.12	0.00	35.46	86.51	ELI-47-20.57-70 13	Chlorite

0.00	0.04	0.08	0.00	33.26	8.57	0.19	0.00	1.52	0.10	0.00	41.90	85.67	ELI-673-20.10 1	Serpentine
0.19	4.52	0.81	0.01	27.46	6.18	0.09	0.02	6.03	0.08	0.01	43.06	88.46	ELI-673-20.10 2	Chl/Amp
0.09	0.00	37.22	0.00	7.95	34.23	0.46	0.01	16.81	0.09	1.21	0.05	98.11	ELI-673-20.10 3	Chlorite
0.04	0.19	6.70	0.00	22.42	37.34	0.30	0.01	5.64	0.08	0.22	23.51	96.44	ELI-673-20.10 4	Chlorite rim
0.42	10.37	0.21	0.00	24.30	3.47	0.17	0.07	0.79	0.06	0.03	57.63	97.52	ELI-673-20.10 5	Amphibole
0.00	0.37	1.42	0.00	30.83	7.68	0.06	0.00	8.47	0.11	0.00	36.73	85.66	ELI-673-20.10 6	Chlorite
0.34	11.71	0.01	0.00	23.55	3.59	0.11	0.03	0.56	0.06	0.01	55.73	95.70	ELI-673-20.10 7	Amphibole
0.00	0.00	35.70	0.00	4.81	38.94	0.87	0.01	14.81	0.12	2.02	0.00	97.28	ELI-673-20.10 8	Chromite
0.01	0.03	9.59	0.00	2.13	76.18	0.37	0.00	0.55	0.03	0.37	2.12	91.39	ELI-673-20.10 8.5	Chromite rim
0.04	17.21	0.13	0.01	22.28	7.03	0.22	0.02	1.67	0.06	0.02	28.33	76.99	ELI-673-20.10 9	Tlc/Crb
0.25	12.91	0.01	0.00	22.47	2.92	0.15	0.02	0.36	0.05	0.02	57.84	96.98	ELI-673-20.10 10	Amphibole
0.00	0.00	31.26	0.00	0.83	47.30	1.39	0.02	12.08	0.07	3.71	0.00	96.65	ELI-675-54.10 1	Chromite
0.06	0.00	29.89	0.02	0.42	54.35	1.05	0.00	7.36	0.10	1.36	0.06	94.67	ELI-675-54.10 2	Chromite rim
0.25	13.31	0.00	0.00	21.99	3.24	0.14	0.01	0.23	0.09	0.00	57.64	96.90	ELI-675-54.10 3	Amphibole
0.00	0.00	0.06	0.02	31.49	11.49	0.16	0.01	1.42	0.08	0.01	41.65	86.39	ELI-675-54.10 4	Serpentine
0.04	0.08	0.30	0.00	27.81	9.63	0.04	0.21	12.49	0.09	0.00	32.71	83.40	ELI-675-54.10 5	Chlorite
0.37	12.70	0.01	0.01	21.90	4.47	0.16	0.02	0.56	0.06	0.03	57.64	97.93	ELI-675-54.10 6	Amphibole
0.00	0.02	0.06	0.00	31.06	11.24	0.10	0.01	3.30	0.07	0.02	40.70	86.58	ELI-675-54.10 7	Serpentine
0.10	0.00	33.97	0.00	4.31	41.77	0.82	0.01	13.17	0.11	2.80	0.05	97.12	ELI-675-54.10 8	Chromite
0.19	0.04	15.02	0.01	10.44	46.13	0.58	0.05	1.56	0.09	0.40	13.50	88.00	ELI-675-54.10 9	Chromite rim
0.37	12.33	0.01	0.00	21.80	3.84	0.18	0.08	0.14	0.02	0.02	57.74	96.53	ELI-675-54.10 10	Amphibole
0.04	0.03	0.74	0.02	31.25	11.71	0.18	0.00	2.32	0.09	0.00	41.44	87.83	ELI-675-54.10 11	Serpentine
0.11	0.04	0.56	0.00	28.73	4.40	0.02	0.02	1.92	0.09	0.02	56.10	92.02	ELI-675-54.10 12	Serpentine
0.42	12.57	0.12	0.01	21.81	3.88	0.20	0.05	0.23	0.01	0.03	57.63	96.95	ELI-675-54.10 13	Amphibole
0.03	0.05	0.60	0.02	30.64	11.61	0.15	0.01	2.71	0.08	0.00	41.38	87.27	ELI-675-54.10 14	Serpentine

Appendix 16. Microprobe analysis results in amphibole pyroxenites.

Na2O	CaO	Cr2O3	P2O5	MgO	FeO	MnO	K2O	Al2O3	NiO	TiO2	SiO2	Total	Sample-Point	Mineral
0.05	0.07	0.12	0.00	26.31	11.90	0.10	0.12	16.17	0.09	0.04	31.14	86.10	ELI-670-52.50 1	Chlorite
0.00	0.02	0.45	0.01	28.55	10.55	0.08	0.02	13.72	0.08	0.00	33.21	86.69	ELI-670-52.50 2	Chlorite
0.45	11.87	0.41	0.02	20.19	6.35	0.33	0.04	0.72	0.01	0.04	56.68	97.09	ELI-670-52.50 3	Amphibole
0.17	11.74	0.07	0.00	21.18	5.75	0.31	0.03	0.28	0.05	0.00	57.84	97.42	ELI-670-52.50 4	Amphibole
0.67	11.64	0.39	0.03	20.46	6.60	0.42	0.02	0.95	0.03	0.05	57.49	98.74	ELI-670-52.50 4.5	Amphibole
0.02	0.03	0.16	0.02	28.50	14.52	0.18	0.02	2.34	0.03	0.01	41.16	86.98	ELI-670-52.50 5	Serpentine
1.03	11.28	0.33	0.03	20.30	7.06	0.34	0.04	1.69	0.06	0.06	56.82	99.03	ELI-670-52.50 6	Amphibole
2.74	12.68	1.22	0.03	15.75	6.68	0.09	1.03	11.84	0.06	4.34	43.96	100.43	ELI-670-52.50 7	K-Pargasite
0.03	0.03	0.27	0.03	28.23	9.80	0.03	0.03	13.39	0.07	0.00	32.78	84.69	ELI-670-52.50 8	Chlorite
0.67	11.24	0.41	0.02	20.47	6.40	0.36	0.08	1.05	0.04	0.02	56.64	97.39	ELI-670-52.50 9	Amphibole
0.22	11.52	0.05	0.01	21.21	5.27	0.25	0.02	0.36	0.03	0.01	57.50	96.45	ELI-670-52.50 10	Amphibole
0.68	12.68	0.22	0.00	20.32	5.79	0.25	0.02	1.09	0.00	0.05	56.92	98.02	ELI-672-34.00 1	Amphibole
0.47	12.83	0.00	0.03	21.89	5.08	0.23	0.01	0.60	0.06	0.02	58.64	99.85	ELI-672-34.00 2	Amphibole
0.04	0.06	0.07	0.04	26.14	12.20	0.04	0.43	16.07	0.11	0.03	31.75	86.98	ELI-672-34.00 3	Chlorite
0.02	0.18	0.14	0.00	27.46	11.52	0.09	0.31	14.57	0.10	0.02	33.96	88.36	ELI-672-34.00 4	Chlorite
0.72	12.36	0.17	0.00	19.72	6.34	0.18	0.02	1.43	0.03	0.07	55.88	96.92	ELI-672-34.00 5	Amphibole
0.48	12.10	0.00	0.00	21.77	4.80	0.24	0.01	0.51	0.02	0.01	57.93	97.87	ELI-672-34.00 6	Amphibole
0.41	12.84	0.00	0.00	21.23	4.50	0.12	0.01	0.53	0.05	0.00	56.94	96.64	ELI-672-34.00 7	Amphibole
0.02	0.00	1.02	0.00	0.13	47.10	1.88	0.01	0.00	0.00	49.03	0.00	99.20	ELI-672-34.00 8	Ilmenite
0.16	12.94	0.03	0.00	22.12	3.36	0.16	0.02	0.24	0.03	0.01	58.66	97.72	ELI-674-73.00 1	Amphibole
0.00	0.08	0.14	0.00	27.42	11.16	0.11	0.12	15.72	0.06	0.03	31.67	86.49	ELI-674-73.00 2	Chlorite
0.36	13.26	0.00	0.01	22.52	3.65	0.23	0.03	0.36	0.08	0.03	59.41	99.94	ELI-674-73.00 3	Amphibole
0.29	12.64	0.01	0.04	21.89	3.81	0.18	0.00	0.26	0.09	0.02	57.97	97.22	ELI-674-73.00 4	Amphibole
0.41	11.74	0.12	0.03	20.75	5.81	0.20	0.01	0.34	0.04	0.04	57.70	97.18	ELI-674-73.00 5	Amphibole
0.65	12.80	0.24	0.00	20.83	5.26	0.20	0.02	1.23	0.04	0.10	56.86	98.21	ELI-674-73.00 6	Amphibole
0.00	0.06	0.09	0.00	27.73	10.86	0.09	0.37	14.92	0.09	0.04	32.65	86.89	ELI-674-73.00 7	Chlorite
0.00	0.03	0.03	0.00	28.14	10.44	0.05	0.09	14.78	0.06	0.01	32.81	86.43	ELI-674-73.00 8	Chlorite
0.36	12.52	0.01	0.00	21.67	4.39	0.27	0.01	0.38	0.06	0.00	57.60	97.28	ELI-674-73.00 9	Amphibole
0.13	13.46	0.01	0.01	22.80	2.74	0.08	0.03	0.19	0.01	0.01	59.37	98.84	ELI-674-73.00 10	Amphibole
0.86	11.57	0.21	0.00	20.41	6.16	0.21	0.05	2.02	0.02	0.04	54.63	96.19	ELI-674-73.00 11	Amphibole
0.87	11.88	0.23	0.00	21.07	6.50	0.21	0.06	1.95	0.04	0.05	55.86	98.71	ELI-674-73.00 12	Amphibole

0.67	11.30	0.14	0.02	20.16	7.20	0.33	0.06	1.38	0.03	0.08	55.08	96.45	ELI-672-45.60-1	Amphibole
0.57	11.93	0.12	0.01	20.99	6.46	0.20	0.01	1.07	0.08	0.04	56.07	97.52	ELI-672-45.60-2	Amphibole
0.14	0.00	0.05	0.01	28.03	11.40	0.09	0.11	15.58	0.11	0.00	31.66	87.17	ELI-672-45.60-3	Chlorite
0.60	11.51	0.26	0.02	20.45	7.38	0.34	0.02	0.93	0.05	0.03	55.85	97.44	ELI-672-45.60-4	Amphibole
0.28	12.10	0.20	0.00	21.13	6.09	0.26	0.02	0.37	0.00	0.01	56.68	97.15	ELI-672-45.60-5	Amphibole
0.06	0.05	0.80	0.00	23.73	11.69	0.15	4.44	13.81	0.10	1.09	33.94	89.85	ELI-672-45.60-6	Phlogopite
0.00	0.02	0.64	0.00	26.63	11.38	0.08	1.46	14.69	0.12	0.15	32.22	87.38	ELI-672-45.60-7	Chl/Phl
0.74	11.75	0.20	0.03	19.97	7.40	0.17	0.05	1.71	0.06	0.14	54.66	96.86	ELI-672-45.60-8	Amphibole
0.47	11.39	0.00	0.01	20.36	7.03	0.39	0.04	0.98	0.08	0.01	55.66	96.42	ELI-672-45.60-9	Amphibole

Appendix 17. Microprobe analysis results in talc pyroxenites.

Na2O	CaO	Cr2O3	P2O5	MgO	FeO	MnO	K2O	Al2O3	NiO	TiO2	SiO2	Total	Sample-Point	Mineral
0.40	11.59	0.00	0.03	21.88	5.82	0.32	0.02	0.40	0.04	0.01	58.12	98.61	R25-3-27 1.1	Amphibole
0.20	3.20	1.08	0.00	5.54	69.61	0.09	0.03	0.30	0.02	0.40	15.29	95.75	R25-3-27 1.2	Magnetite
0.47	11.36	0.10	0.02	21.45	5.55	0.29	0.03	0.47	0.03	0.07	58.09	97.92	R25-3-27 1.3	Amphibole
0.22	0.05	0.22	0.00	27.86	4.87	0.06	0.09	1.78	0.07	0.02	58.02	93.27	R25-3-27 1.4	Talc
0.97	11.03	0.40	0.01	20.69	6.30	0.26	0.05	1.39	0.03	0.09	56.26	97.49	R25-3-27 2	Amphibole
0.57	0.01	0.27	0.01	28.70	4.24	0.04	0.08	1.13	0.07	0.05	61.64	96.80	R25-3-27 2.5	Talc
0.63	11.75	0.01	0.00	20.33	6.24	0.30	0.07	0.73	0.04	0.00	55.58	95.66	R25-3-27 2R	Amphibole
0.05	0.00	0.03	0.00	27.94	10.96	0.03	0.37	14.52	0.04	0.02	33.36	87.31	R25-3-27 4	Chlorite
0.32	0.00	0.33	0.00	28.28	4.35	0.02	0.07	1.51	0.05	0.03	58.74	93.72	R25-3-27 3	Talc
0.47	11.53	0.09	0.00	21.87	5.30	0.26	0.03	0.49	0.02	0.01	57.86	97.93	R25-3-27 3.5	Amphibole
0.11	0.00	0.75	0.00	26.64	12.20	0.30	0.55	12.50	0.05	4.32	31.41	88.83	R25-3-27 10	Chlorite
0.12	0.04	0.79	0.01	20.82	12.83	0.20	5.97	12.21	0.05	4.60	34.19	91.81	R25-3-27 10.5	Phlogopite
0.05	0.06	0.02	0.00	28.47	11.00	0.08	0.41	12.74	0.07	0.02	35.37	88.28	R25-3-27 7	Chlorite
0.04	0.00	0.00	0.00	26.45	11.29	0.12	0.26	17.22	0.07	0.03	30.84	86.30	R25-3-27 8	Chlorite

Appendix 18. Microprobe analysis results in serpentinites.

Na2O	CaO	Cr2O3	P2O5	MgO	FeO	MnO	K2O	Al2O3	NiO	TiO2	SiO2	Total	Sample-Point	Mineral
0.07	0.00	42.12	0.00	10.12	26.16	0.36	0.00	18.00	0.12	0.69	0.02	97.66	ELI-731-147.45-50 1	Chromite
0.22	0.00	1.43	0.02	5.51	79.56	0.34	0.05	0.15	0.74	0.05	2.59	90.67	ELI-731-147.45-50 2	Chromite rim
0.34	0.00	41.36	0.00	9.22	28.31	0.44	0.08	18.75	0.10	0.75	0.01	99.36	ELI-731-147.45-50 3	Chromite
0.75	0.01	5.65	0.01	6.41	64.76	0.90	0.15	0.20	0.21	0.08	4.19	83.32	ELI-731-147.45-50 4	Chromite rim
0.04	0.00	0.04	0.00	39.84	1.23	0.04	0.02	1.16	0.10	0.04	44.35	86.86	ELI-731-147.45-50 5	Serpentine
0.51	0.03	0.02	0.00	39.79	3.13	0.06	0.21	0.00	0.24	0.00	39.61	83.60	ELI-731-147.45-50 6	Serpentine
0.02	0.00	0.80	0.00	0.83	88.06	0.22	0.01	0.03	0.68	0.09	0.15	90.88	ELI-731-147.45-50 7	Magnetite
0.07	0.01	42.92	0.03	9.49	27.90	0.40	0.03	17.15	0.12	0.81	0.00	98.92	ELI-731-147.45-50 8	Chromite
0.00	0.00	4.90	0.00	1.30	84.26	0.34	0.01	0.18	0.59	0.31	0.03	91.91	ELI-731-147.45-50 9	Chromite rim
0.04	0.02	0.01	0.00	38.58	1.92	0.07	0.02	2.00	0.07	0.04	42.47	85.24	ELI-731-147.45-50 10	Serpentine
0.28	0.02	0.00	0.00	38.17	4.99	0.06	0.09	0.00	0.13	0.03	36.04	79.81	ELI-731-147.45-50 11	Serpentine